PROPOSED MINIMUM RESTORING FORCE EQUATIONS FOR SEISMIC ISOLATED STRUCTURES

A THESIS SUBMITTED TO
THE GRADUATE SCHOOL OF NATURAL AND APPLIED SCIENCES
OF
MIDDLE EAST TECHNICAL UNIVERSITY

BY

ALİ GÜNALP GÖRGÜLÜ

IN PARTIAL FULFILLMENT OF THE REQUIREMENTS
FOR
THE DEGREE OF MASTER OF SCIENCE
IN
ENGINEERING SCIENCES

DECEMBER 2019

Approval of the thesis:

PROPOSED MINIMUM RESTORING FORCE EQUATIONS FOR SEISMIC ISOLATED STRUCTURES

submitted by **ALİ GÜNALP GÖRGÜLÜ** in partial fulfillment of the requirements for the degree of **Master of Science in Engineering Sciences Department, Middle East Technical University** by,

Prof. Dr. Halil Kalıpçılar
Dean, Graduate School of **Natural and Applied Sciences** ________________

Prof. Dr. Murat Dicleli
Head of Department, **Engineering Sciences** ________________

Prof. Dr. Murat Dicleli
Supervisor, **Engineering Sciences, METU** ________________

Examining Committee Members:

Prof. Dr. Murat Altuğ Erberik
Civil Engineering, METU ________________

Prof. Dr. Murat Dicleli
Engineering Sciences, METU ________________

Prof. Dr. Tolga Akış
Civil Engineering, Atılım University ________________

Date: 11.12.2019

I hereby declare that all information in this document has been obtained and presented in accordance with academic rules and ethical conduct. I also declare that, as required by these rules and conduct, I have fully cited and referenced all material and results that are not original to this work.

Name, Surname: Ali Günalp Görgülü

Signature:

ABSTRACT

PROPOSED MINIMUM RESTORING FORCE EQUATIONS FOR SEISMIC ISOLATED STRUCTURES

Görgülü, Ali Günalp
Master of Science, Engineering Sciences
Supervisor: Prof. Dr. Murat Dicleli

December 2019, 58 pages

In this research study, a new set of restoring force equations are proposed for seismic isolated structures subjected to far fault ground motions (FFGM) and near fault ground motions (NFGM). For this purpose, 110 FFGM and 49 NFGM are selected. Then, nonlinear time history analyses (NLTHA) of SDOF seismic isolated structures are performed using the selected ground motions to obtain their residual and maximum displacements. The analyses are repeated for an extensive range of parameters including peak ground acceleration, A_p, characteristic strength, Q_d and post elastic period, T_d, of the isolation system. Next, the variations of the residual and maximum displacements are plotted as functions of the various combinations of the parameters considered in the analyses. Then, nonlinear regression analyses are performed to formulate the residual and maximum displacements as functions of the parameters considered in the analyses. The developed equations are then used to formulate the upper limits of T_d (restoring force equations) to ensure reasonable levels of residual and maximum isolator displacements. The developed restoring force equations are then compared with those of AASHTO [1] and Eurocode-8 (EC-8) [2] using the pool of residual and maximum displacement data obtained from NLTHA. It is observed that unreasonably large levels of residual and maximum displacements may be obtained for some cases when the restoring force equations of AASHTO [1] and EC-8 [2] are used. However, when the restoring force requirements proposed in this research study are applied, the residual and maximum displacements are observed to be within feasible ranges.

Keywords: Maximum and Residual Displacement, Restoring Force Requirement, Non-linear Time History Analysis, Seismic Isolated Structure, Near and Far Fault Ground Motions

ÖZ

SİSMİK YALITIMLI YAPILAR İÇİN ÖNERİLEN MİNİMUM MERKEZLEME DENKLEMLERİ

Görgülü, Ali Günalp
Yüksek Lisans, Mühendislik Bilimleri
Tez Danışmanı: Prof. Dr. Murat Dicleli

Aralık 2019, 58 sayfa

Bu tez çalışmasında, uzak ve yakın saha deprem hareketlerine maruz kalan deprem yalıtımlı yapılar için merkezleme denklemleri önerilmiştir. Bunun için 110 adet uzak saha deprem kaydı ve 49 adet yakın saha deprem kaydı seçilmiştir. Daha sonra, tek serbest dereceli ve deprem yalıtımlı yapı modellerinin, seçilen deprem kayıtlarının doğrusal olmayan zaman serisi yöntemiyle analiz edilmesi sonucunda kalıcı ve maksimum deplasmanlar elde edilmiştir. Analizler, maksimum yer ivmesi, A_p , karakteristik mukavemet, Q_d, ve elastik ötesi peryot, T_d parametrelerine bağlı olarak tekrarlanmıştır. Ardından, kalıcı ve maksimum sistem deplasmanlarının bu parametrelere göre değişimleri grafiklerle incelenmiştir. Sonrasında, kalıcı ve maksimum deplasmanları formülize etmek amacıyla lineer olmayan regresyon analizleri yapılmıştır. Bulunan formüller kullanılarak makul kalıcı ve maksimum deplasmanlar elde etmek için gerekli olan en büyük elastik ötesi peryotlar formülize edilmiştir. Bulunan merkezleme formülleri, analiz sonuçları da kullanılarak AASHTO [1] ve EC-8[2] kodlarıyla karşılaştırılmıştır. Bahsi geçen kodların merkezleme denklemleri kullanıldığında bazı durumlarda makul olmayan büyüklükte kalıcı ve maksimum deplasmanlar bulunmuştur. Fakat bu çalışmada önerilen formüller kullanıldığında ise kalıcı ve maksimum yalıtım sistemi deplasmanlarının makul seviyelerde bulunduğu gözlemlenmiştir.

Anahtar Kelimeler: Maksimum ve Kalıcı Deplasmanlar, Merkezleme Şartları, Doğrusal Olmayan Zaman Serisi Analizi, Sismik Yalıtımlı Yapı, Yakın ve Uzak Saha Depremleri

To my wife

ACKNOWLEDGEMENTS

First and foremost, I would like to thank to my supervisor, Prof. Dr. Murat DİCLELİ for his great support, guidance and patience during my study. He made special effort to allocate time for this study despite his busy schedule. Moreover, he was always very kind to me and encouraged me to finish this research on time.

I would like to express my admiration to my lovely wife Yaşam Görgülü. Her support and courage have inspired me from the first day of this study. Whenever I feel depressed, she pointed out the light at the end of the tunnel.

I am also grateful to my family. My parents, Osman Görgülü and Ayşe Görgülü have motivated me throughout my life. I am also thankful to my father in law Hasan Kızıldağ and mother in law Canan Kızıldağ for their great support.

A very special thanks go to my dear sisters Günseli and Gülşen and to my smart and pretty nephews Umut Erdem, Mustafa Ege and Onuralp. I will be forever grateful for their presence in my life.

TABLE OF CONTENTS

LIST OF TABLES

TABLES

LIST OF FIGURES

FIGURES

LIST OF ABBREVIATIONS

ABBREVIATIONS

AASHTO: American Association of State Highway and Transportation Officials

ASCE: American Society of Civil Engineers

Avg: Average

EC-8: Eurocode 8

FFGM: Far Fault Ground Motions

FWHA: Federal Highway Administration

LRFD: Load Resistance Factor Design

NFGM: Near Fault Ground Motions

NHI: National Highway Institute

NLTHA: Nonlinear Time History Analysis

PEER: Pacific Earthquake Engineering Research Center

SDOF: Single Degree of Freedom

LIST OF SYMBOLS

SYMBOLS

A_p: Average Peak Ground Acceleration

d_{max}: Maximum Displacement

d_{res}: Residual Displacement

d_{rm}: Static Residual Displacement

E_h: Energy Dissipated by Hysteric Deformation

E_s: Reversibly Stored Energy

F_y: Yield Strength

g: Gravitational Acceleration

k_d: Post Elastic Stiffness

k_i: Initial or Elastic Stiffness

m: Mass

M_w: Moment Magnitude

Q_d: Characteristic Strength

R: Closest Distance to Rupture Plane

R^2: Coefficient of Determination

S_a: Spectral Acceleration

T: Period

T_c: Second Corner Period

T_d: Post Elastic Period

T_p: Average Pulse Period

V_p: Average Peak Ground Velocity

W: Weight

u: Displacement

$\dot{u}$: Velocity

$\ddot{u}$: Acceleration

CHAPTER 1

INTRODUCTION

1.1. Introduction

Seismic isolation of structures is a simple design approach where isolators are interposed between the superstructure and foundation/substructure to decouple the superstructure from the effect of ground shaking by yielding or sliding of the isolators. In the last two decades, the use of this force mitigation technology has become quite popular. Parallel to the developments of the seismic isolation technology, design specifications have evolved to ensure safety and serviceability of seismic isolated structures before, during and after a potential earthquake. Seismic isolators generally have a bilinear force-displacement relationship. The second slope of this relationship, the post-elastic stiffness, is responsible for providing restoring force capability to the seismic isolation system so as to achieve reasonable levels of maximum and residual displacements during and after an earthquake respectively. It is a known fact that properly designed seismic isolated structures may survive a design-basis earthquake with little or no damage to their load-bearing structural systems. A properly designed seismic isolation system involves minimizing the maximum and residual isolation system displacements while keeping the base shear and floor accelerations at reasonable levels to ensure continued functionality of the structure. If the isolation system lacks adequate restoring force capability, large residual displacements may remain in the isolation system after a potential earthquake. Such residual displacements may result in elevation differences at the seismic joints affecting the serviceability of the structure. For instance, in the case of curved surface sliders the superstructure will go up or in the case of high damping or lead rubber bearings it will go down. Furthermore, excessive isolator displacements may result in large costs since larger isolation bearings and seismic joints are needed to withstand large displacements. Another concern is the large cumulative displacements of the isolation system originating from aftershocks due to lack of proper restoring force capability. Therefore, maximum and residual displacements in isolators should be kept under control by providing an adequate restoring force capability.

Design specifications for seismic isolated structures such as AASHTO [1], ASCE 7-16 [3], EN15129 [4] and EC-8 [2] provide some requirements to ensure adequate restoring force capability of the isolation system. AASHTO's [1] minimum restoring force capability requirement is based on restricting the residual and maximum displacements using two equations, one of which is a function of the maximum isolation system displacement, post elastic stiffness and superstructure weight and the other is a function of the post-elastic period (a period calculated using the superstructure weight and post elastic stiffness of the isolation system). ASCE-7-16 [3] is similar to AASHTO [1], but only employs the first approach in a more restrictive way to ensure reasonable levels of residual displacements. EC-8[2] on the other hand, warrants an adequate isolation system restoring force capability solely based on restricting the residual displacements, while EN15129 [4] bases its restoring force requirement on the ratio of the elastic or potential energy to the hysteretic energy of the isolation system.

Involving the maximum isolator displacement while checking the restoring force capability of an isolations system is not practical since the maximum displacement cannot be predicted unless the properties of the seismic isolation system including the post-elastic stiffness is already defined and a seismic analysis for the structure is performed. Furthermore, the maximum and residual displacement of an isolation system is a function of the characteristic strength, post elastic period as well as the characteristics of the ground motion such as the peak ground acceleration and frequency content. Thus, the restoring force requirements should also explicitly employ the aforementioned parameters to check the adequacy of the restoring force capability of any seismic isolation system. In addition, the restoring force requirements of the current seismic isolation design codes do not differentiate between

Far Fault Ground Motions (FFGM) and Near Fault Ground Motions (NFGM). As NFGM with forward rupture directivity effect contain intense, long duration velocity pulses, the restoring force requirements of seismic isolated structures subjected to such ground motions should be more restrictive to avoid large residual and maximum displacements to ensure the continued functionality of the structure.

Several researchers have investigated the concept of restoring force capability for seismic isolated structures. Medeot [5] used an energy approach to define the minimum restoring force requirement of isolation systems. Tsopelas et al. [6] on the other hand, derived a formula to limit the residual displacements of the isolation system where the characteristic strength was used as a parameter and the research results were compared with the requirements of AASHTO [7]. Katsaras et al. [8] also derived a similar equation focusing on limiting the residual displacements where the research results were compared with the restoring force requirements of AASHTO [9]. Cardone et al. [10] obtained an equation with parameters similar to that of Katsaras et al. [8], but recommending the use of a more restrictive formula to obtain reasonable levels of residual isolator displacements independent of the ground motion characteristics. The above-mentioned research studies are based on only limiting the residual displacements. Furthermore, the proposed equations are functions of the maximum and static residual displacements where the effect of the distance to fault (far-fault vs. near-fault) as well as the intensity and frequency characteristics of the ground motion are ignored. Furthermore, although the static residual displacement is defined as the ratio of the characteristic strength to post elastic stiffness of the isolation system, with such an approach, the independent effects of these parameters, on the restoring force requirement cannot be considered. Accordingly, a research study is urgently needed to develop new equations to limit both the residual and maximum isolation system displacements for the cases of FFGM and NFGM as functions of the isolator properties and ground motion characteristics.

1.2. Research Objective, Scope and Outline

The main objective of this research study is to develop equations for providing adequate restoring force capability by imposing an upper limit to the post-elastic period of seismic isolation systems to ensure reasonable levels of residual and maximum isolator displacements. Two sets of equations will be developed; one set for FFGM and another set for NFGM. The developed equations will be functions of both isolator and ground motion characteristics. The developed sets of equations are expected to address the shortages in current seismic isolation design codes where the code equations are developed considering solely FFGM and do not include the independent effect of seismic isolation system parameters as well as ground motion characteristics such as intensity and frequency content. Furthermore, most seismic isolation design codes, except AASHTO [1], consider minimum restoring force requirements of seismic isolations systems solely based on ensuring reasonable levels of residual displacements neglecting the requirement to control the level of maximum isolator displacements.

The scope of this research study is limited to seismic isolation systems with bilinear force-displacement behavior. The set of equations developed as part of this research study to ensure adequate restoring force capability are based on the Nonlinear Time History Analysis (NLTHA) results of SDOF seismic isolated structures.

The outline of this research is as follows;

1. First, 110 FFGM and 49 NFGM records are selected from the PEER [11] (Pacific Earthquake Engineering Research Center) database and the database provided by Baker [12] respectively. FFGM are divided into 10 groups by their A_p/V_p (peak ground acceleration to peak ground velocity) ratios and NFGM are divided into seven groups by their T_p (velocity pulse period). The average of the NLTHA results performed in the subsequent steps of the research study for each group is then used to relate the analyses results to the frequency

characteristics of the ground motion (Average of A_p/V_p for FFGM and T_p for NFGM).

2. Then, SDOF seismic isolated structures with a single tributary mass placed on an isolator with a bilinear force-displacement relationship are modelled in the structural analysis software SAP2000 [13]. Next, NLTHA of the SDOF models are conducted for the selected groups of ground motions where each group reflects a certain frequency level of the ground motion (Average of A_p/V_p for FFGM and T_p for NFGM). The analyses are repeated for an extensive range of parameters including peak ground acceleration, A_p, characteristic strength, Q_d and post elastic period, T_d, which is calculated using the post-elastic stiffness, k_d, of the isolator. This resulted in a total of 101760 analyses cases (70400 analyses cases for FFGM and 31360 cases for NFGM). From the analyses results, the average of the residual and maximum displacements for each group of ground motions are obtained and recorded.

3. Next, the variations of the residual and maximum displacements are plotted as functions of the various combinations of the parameters considered in the analyses. Then, nonlinear regression analyses are performed to formulate the residual and maximum displacements as functions of the parameters considered in the analyses, which are; mA_p, Q_d, T_d and A_p/V_p for FFGM as well as mA_p, Q_d, T_d and T_p for NFGM.

4. The residual and maximum displacement equations obtained in the previous step contain the average A_p/V_p from each group of 11 FFGM and average T_p from each group of seven NFGM. These parameters are not feasible to use in practice since only the design response spectrum is available to the designer. Consequently, additional studies are performed to obtain equations that relate the A_p/V_p for FFGM and T_p for NFGM to the second corner period of the design response spectrum, T_c. The formulated equations are also verified by using a

different set of ground motions. These relationships are then substituted in place of the A_p/V_p for FFGM and T_p for NFGM to obtain the final simplified form of the residual and maximum displacement equations.

5. This step involves the development of the upper limits of T_d (minimum restoring force requirement) to ensure reasonable levels of residual and maximum isolator displacements using the developed residual and maximum displacement equations and the NLTHA results for the entire pool of data. As a result, in total four equations for T_d are derived, two for FFGM and two for NFGM, to ensure reasonable levels of residual and maximum isolator displacements.

6. In the final step of the research study, the restoring force requirements of the current design codes together with the restoring force equations developed as part of this study are first compared and assessed using the NLTHA data. Next, inadequacy of the current design codes is presented for the cases where the residual and maximum isolator displacements reach unfeasible levels even if the code requirements are satisfied. At the end, it is shown that the restoring force requirements developed as part of this study ensure reasonable levels of residual and maximum isolator displacements for a wide range of isolator and ground motion properties.

CHAPTER 2

ANALYSIS MODEL AND PROPERTIES OF TYPICAL SEISMIC ISOLATORS

The force-displacement hysteretic relationship of a typical isolation system is generally idealized by a bi-linear function as shown in Figure 2.1(a). In the figure, Q_d is the characteristic strength, F_y is the yield strength, k_i is the initial or elastic stiffness, k_d is the post-elastic stiffness, d_{max} is the maximum isolator displacement, d_{res} is the residual displacement and d_{rm} is the maximum static residual displacement, which may be computed as Q_d/K_d from the geometry of the hysteresis loop. A SDOF system shown in Figure 2.1(b) is modelled in SAP2000 [13] to estimate the residual and maximum isolator displacements for a wide range of isolator and ground motion properties. The idealized bilinear force-displacement hysteretic behavior of the seismic isolation system shown in Figure 2.1(b) is modeled using a nonlinear link element (Wen Plasticity property). In the model, one end of the nonlinear link element (NLINK) is fixed and the other end is attached to a single mass of 2000kN resting on a roller support.

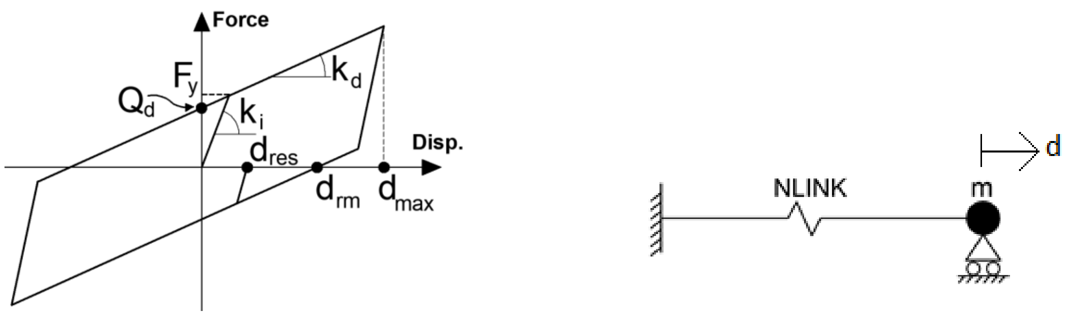

(a) (b)

Figure 2.1.(a) Idealized bi-linear force displacement relationship of isolation system (b) SDOF model

It is noteworthy that in the NLTHA, the total time of the acceleration record is extended to an extra 2% of the total time of the record to correctly estimate the residual displacements at the end of an earthquake.

The equation of motion for linear analysis is as follows;

$$Ku(t) + C\dot{u}(t) + M\ddot{u}(t) = -m\ddot{u}_g(t) \qquad (1)$$

where K is the stiffness matrix, C is the damping matrix, M is the mass matrix, t is time; u, $\dot{u}$ and $\ddot{u}$ are the displacements, velocities and accelerations of the structure respectively. In this study, NLTHA is performed. For this type of analysis, $Ku(t)$ term is replaced by $F(u)$ in Eq.1

CHAPTER 3

RESTORING FORCE REQUIREMENT IN THE LITERATURE AND CURRENT DESIGN CODES

In this part, the requirements presented by academic researches and the current design codes are investigated about the restoring force capability concept.

Tsopelas et al. [6] proposed that, the ratio of characteristic strength to the restoring force at design displacement should be smaller than 3.0 to get a sufficient restoring force capability for an isolated system. In other words, d_{max}/d_{rm} is required to be greater than 0.33.

Kawashima et al. [14] developed a residual displacement response spectrum and concluded that the residual displacements are significantly dependent on the ratio of the post-elastic stiffness to the initial stiffness of the isolation system. The approach of Kawashima et al. [14] is also based on limiting the residual displacement of seismic isolation systems. However, such an approach is mostly suitable for rubber-based isolation systems where the initial or elastic slope is better defined but it is impractical for seismic isolation systems based on sliding behavior. The initial stiffness of sliding isolation systems is very large and not readily available to the designer.

Medeot [5] suggested a theoretical approach to self-centering problem and presented energy concept to explain self-centering capability of an isolator by deriving the equation of $E_S \geq 0.25E_H$ where E_S is the reversibly stored energy and E_H is the energy dissipated by hysteretic deformation.

Katsaras et al. [8] suggested that the concept of restoring force capability should not be based only on the parameters of the isolation system but also on the properties of the seismic activity, which is related to the maximum displacement of the isolation system. Accordingly, the ratio, d_{max}/d_{rm} (the ratio of maximum displacement to static residual displacement) is presented as the main parameter affecting the restoring force capability of an isolation system and this ratio is proposed to be greater than 0.5 to achieve reasonable levels of restoring force capability.

Cardone et al. [10] investigated the concept of restoring force capability of friction pendulum seismic isolation systems and concluded that an adequate re-centering capability is achieved, regardless of the characteristic of the ground motion, if d_{max}/d_{rm} ratio is greater than 2.5. Moreover, an equation is derived to calculate the residual displacements for friction pendulum systems subjected to FFGM. The developed equation is then multiplied by some coefficients to obtain the residual displacements for NFGM.

The AASHTO Guide Specifications for Seismic Isolation Design [1] presents two restoring force requirements. The first one is based on limiting the residual displacements and requires that $\Delta F \geq 0.0125W$, where W is the weight of the system and ΔF is the difference between the forces at design displacement (d_{max}) and 50% of the design displacement ($0.5d_{max}$). The mathematical representation of this requirement may be presented in a different form as follows,

$$\frac{k_d\ d_{max}}{W} > 0.025 \tag{2}$$

The second requirement of AASHTO [1] states that the post-elastic period (T_d) of the seismic isolation system (calculated based on the post elastic stiffness (k_d)) should be smaller than 6.0 seconds;

$$T_d < 6\ s \tag{3}$$

By solving Eqs.2 and 3 simultaneously and knowing that $T_d = 2\pi\sqrt{\frac{m}{k_d}}$, the following formula is derived,

$$2\pi\sqrt{\frac{d_{max}}{0.025\ g}} < \ 6\ s \tag{4}$$

By solving Eq.4 for d_{max}, it may be concluded that the maximum isolation system displacement is limited to 224 mm (approx. 9 inches) in AASHTO [1]. This derivation is also available in the reference manual "LRFD Seismic Analysis and Design of Bridges - FHWA-NHI-15-004 [15]. Furthermore, Q_d is not considered as a parameter for restoring force capability in AASHTO.

The restoring force requirement of ASCE 7-16 [3] is similar to the first rule of AASHTO [1], where the condition $\Delta F \geq 0.025W$ should be satisfied. However, this condition requires a minimum restoring force twice that of AASHTO [1].

According to Eurocode 8 [2], the ratio, d_{max}/d_{rm} should be greater than 0.5 to ensure adequate lateral restoring capability for seismic isolated systems. That is;

$$\frac{d_{max}}{d_{rm}} > 0.5 \tag{5}$$

Except AASHTO [1], the restoring force requirements proposed by the above-mentioned researchers, ASCE 7-16 [3] and Eurocode 8 [2] are all based on limiting only the residual displacements. In addition, most of the restoring force requirements in the literature and the design codes require the calculation of the design or maximum displacement, which is not available to the designer at the initial design stage, to check the restoring force capability of seismic isolation systems. Moreover, the minimum restoring force requirements proposed in the literature and design codes discussed above do not differentiate between FFGM and NFGM and do not explicitly consider the effect of isolator and ground motion properties.

CHAPTER 4

PARAMETERS AND GROUND MOTIONS CONSIDERED IN THE ANALYSIS

4.1. Parameters Considered in The Analysis

Residual and maximum displacements as well as the restoring force capability of an isolation system may be affected by both isolator and ground motion characteristics. Thus, in this research study, mA_p, A_p/V_p ratio for FFGM and T_p for NFGM are considered as parameters representing the characteristics of the ground motion and Q_d and T_d are considered as parameters representing the properties of the seismic isolation system.

In the NLTHA, the weight of the SDOF seismic isolation systems is selected as 2000 kN, while the peak ground acceleration, A_p is assumed to have the following range of values; 0.2g, 0.4g, 0.6g, 0.8g, 1.0g, 1.2g, 1.4g and 1.6g. The groups of FFGM considered in the analyses are chosen to have average A_p/V_p ratios ranging between 5.2 and 27.2 s^{-1} while the groups of NFGM considered in the analyses are chosen to have average T_p values ranging between 0.70 s and 8.67 s. More detailed information about the ground motions used in the analyses is given in the subsequent section. Eight different values of characteristic strength Q_d in terms of the structure weight, W are considered as follows; 0.02W, 0.04W, 0.06W, 0.08W, 0.10W, 0.12W, 0.14W and 0.16W while the post elastic period of the isolation system is assigned 10 different values ranging between 1s and 10s at 1s increments.

Accordingly, $8 \times 8 \times 10 = 640$ analyses cases are considered for a single ground motion record. In total, NLTHA of $640 \times 110 = 70400$ and $640 \times 49 = 31360$ different cases are performed for FFGM and NFGM respectively. Moreover, mA_p/Q_d is a rational parameter representing the ratio of the seismic force on a rigid structure to the characteristic strength of the system. The values of this parameter used in this research study are summarized in Table 4.1. In this table, this dimensionless parameter varies between 1.25 and 80.

Table 4.1. *Range of mA_p/Q_d values considered in the analyses*

Q_d	A_p							
	0.2g	0.4g	0.6g	0.8g	1.0g	1.2g	1.4g	1.6g
0.02W	10.00	20.00	30.00	40.00	50.00	60.00	70.00	80.00
0.04W	5.00	10.00	15.00	20.00	25.00	30.00	35.00	40.00
0.06W	3.33	6.67	10.00	13.33	16.67	20.00	23.33	26.67
0.08W	2.50	5.00	7.50	10.00	12.50	15.00	17.50	20.00
0.10W	2.00	4.00	6.00	8.00	10.00	12.00	14.00	16.00
0.12W	1.67	3.33	5.00	6.67	8.33	10.00	11.67	13.33
0.14W	1.43	2.86	4.29	5.71	7.14	8.57	10.00	11.43
0.16W	1.25	2.50	3.75	5.00	6.25	7.50	8.75	10.00

4.2. Ground Motions Considered in The Analysis

The 110 FFGM considered in this research study are listed in Table 4.2. The ground motions are selected from the "New NGA-West 2 Database" provided by PEER [11] (Pacific Earthquake Engineering Research Center). The FFGM are chosen among those with R (closest distance to earthquake rupture plane) ranging between 20 and 60 km (to represent FFGM characteristics and have reasonable levels of A_p) and having moment magnitudes (M_W) larger than 5.5. The ground motions are then grouped into 10 bins of 11 records according to their A_p/V_p ratio ranging between 4.9 and 42.2 s^{-1}. The average A_p/V_p ratio of the groups of FFGM range between 5.2 and 27.2 s^{-1}.

The 49 NFGM considered in this research study are listed in Table 4.3. The ground motions are selected from the database provided by Baker [12] where NFGM are selected from PEER database and the orthogonal (to fault) components of these ground motions are distinguished to represent directivity. Baker [12] used wavelet analysis to obtain pulse periods for each ground motion. After selecting ground motions from Baker's [12] database, the ground motions are then grouped into seven bins of seven records according to their T_p ranging between 0.4 s and 9.1 s. The average T_p of the groups of NFGM range between 0.70 s and 8.67 s.

Table 4.2. *Selected FFGM Records*

Gr.no	No	Event	Station	M_W	R (km)	A_p/V_p (s^{-1})	Avg. A_p/V_p (s^{-1})
1	1	Borrego Mtn	El Centro Array #9	6.6	46	4.9	**5.2**
	2	Landers	Thousand Palms Post Office	7.3	37	4.9	
	3	Chi-Chi, Taiwan-04	CHY027	6.2	54	4.9	
	4	El Mayor-Cucapah, Mexico	Rock Hill	7.2	58	5	
	5	L'Aquila, Italy	Avezzano	6.3	27	5.1	
	6	Chi-Chi, Taiwan-04	TCU140	6.2	53	5.1	
	7	Chi-Chi, Taiwan-04	CHY088	6.2	48	5.3	
	8	Kocaeli, Turkey	Atakoy	7.5	58	5.3	
	9	Darfield, New Zealand	Hulverstone Drive Pump. St.	7.0	25	5.5	
	10	Parkfield-02, CA	Monarch Peak	6	29	5.6	
	11	El Mayor-Cucapah, Mexico	Holtville Post Office	7.2	37	5.6	
2	12	El Mayor-Cucapah, Mexico	TAMAULIPAS	7.2	27	5.8	**6.5**
	13	Morgan Hill	Agnews State Hospital	6.2	24	5.9	
	14	El Mayor-Cucapah, Mexico	Westmorland Fire Sta	7.2	43	6.3	
	15	El Mayor-Cucapah, Mexico	Meloland, E Holton Rd.	7.2	31	6.5	
	16	Big Bear-01	San Bernardino – E & Hosp.	6.5	35	6.6	
	17	Chi-Chi, Taiwan-04	TCU051	6.2	56	6.6	
	18	Gulf of Aqaba	Eilat	7.2	44	6.6	
	19	Darfield, New Zealand	Pages Road Pumping Station	7.0	25	6.6	
	20	Chi-Chi, Taiwan-04	TCU119	6.2	55	6.6	
	21	Chi-Chi, Taiwan-04	CHY015	6.2	50	6.8	
	22	Landers	Palm Springs Airport	7.3	36	6.9	
3	23	El Mayor-Cucapah, Mexico	Salton Sea Wildlife Refuge	7.2	58	7	**7.5**
	24	Imperial Valley-06	El Centro Array #13	6.5	22	7.2	
	25	Darfield, New Zealand	SBRC	7.0	24	7.2	
	26	Kobe, Japan	Yae	6.9	28	7.3	
	27	Chi-Chi, Taiwan-04	TCU145	6.2	56	7.4	

Table 4.2. *(Continued)*

Gr.no	No	Event	Station	M_W	R (km)	A_p/V_p (s^{-1})	Avg. A_p/V_p (s^{-1})
	28	El Mayor-Cucapah, Mexico	Bonds Corner	7.2	33	7.5	
	29	Darfield, New Zealand	WSFC	7.0	27	7.6	
	30	Kocaeli, Turkey	Zeytinburnu	7.5	54	7.6	
	31	El Mayor-Cucapah, Mexico	El Centro Meadows Union Sch.	7.2	28	7.7	
	32	Kobe, Japan	Morigawachi	6.9	25	7.8	
	33	Darfield, New Zealand	DORC	7.0	33	7.8	
4	34	Chi-Chi, Taiwan-04	CHY101	6.2	22	7.9	8.6
	35	Imperial Valley-06	Calipatria Fire Station	6.5	25	8.1	
	36	Morgan Hill	Hollister Differential Array #3	6.2	26	8.1	
	37	Landers	Indio – Jackson Road	7.3	49	8.4	
	38	Landers	Desert Hot Springs	7.3	22	8.6	
	39	Imperial Valley-06	Delta	6.5	22	8.8	
	40	Darfield, New Zealand	Kaiapoi North School	7.0	31	8.8	
	41	Hector Mine	Desert Hot Springs	7.1	56	8.8	
	42	Imperial Valley-06	Niland Fire Station	6.5	37	8.8	
	43	Imperial Valley-06	Coachella Canal #4	6.5	50	8.9	
	44	El Mayor-Cucapah, Mexico	El Centro – Meloland Geotech.	7.2	29	8.9	
5	45	Denali, Alaska	R109 (temp)	7.9	43	9.1	9.6
	46	Morgan Hill	Hollister City Hall	6.2	31	9.1	
	47	El Mayor-Cucapah, Mexico	El Centro Array #4	7.2	35	9.2	
	48	Kobe, Japan	Sakai	6.9	28	9.4	
	49	Bam, Iran	Mohammad Abad-e-Madkoon	6.6	46	9.5	
	50	Kocaeli, Turkey	Fatih	7.5	55	9.6	
	51	Big Bear-01	Joshua Tree	6.5	42	9.7	
	52	Chi-Chi, Taiwan-04	CHY019	6.2	54	9.8	
	53	Big Bear-01	Rancho Cucam. Law& Just. Cntr. FF	6.5	60	10.1	
	54	Chi-Chi, Taiwan-04	CHY087	6.2	38	10.1	
	55	Kozani, Greece-01	Veroia (bsmt)	6.4	57	10.2	
6	56	Morgan Hill	San Justo Dam (R Abut)	6.2	32	10.2	10.6
	57	L’Aquila, Italy	Mompeo 1	6.3	49	10.2	
	58	Sitka, Alaska	Sitka Observatory	7.7	35	10.3	
	59	Big Bear-01	North Palm Spr. Fire Sta #36	6.5	42	10.85	

Table 4.2. *(Continued)*

Gr.no	No	Event	Station	M_W	R (km)	A_p/V_p (s^{-1})	Avg. A_p/V_p (s^{-1})
	60	Chi-Chi, Taiwan-04	HWA037	6.2	52	10.5	
	61	Chi-Chi, Taiwan-04	HWA041	6.2	50	10.5	
	62	Kozani, Greece-01	Veroia (bsmt)	6.4	57	10.8	
	63	Landers	Forest Falls Post Office	7.3	45	10.7	
	64	Darfield, New Zealand	PEEC	7.0	54	10.7	
	65	L'Aquila, Italy	Mompeo 1	6.3	49	10.8	
	66	Irpinia, Italy-02	Brienza	6.2	43	10.8	
7	67	Chi-Chi, Taiwan-04	HWA039	6.2	50	10.8	**11.2**
	68	Morgan Hill	San Justo Dam (L Abut)	6.2	32	10.9	
	69	L'Aquila, Italy	Ortucchio	6.3	37	10.9	
	70	Chi-Chi, Taiwan-04	CHY052	6.2	45	11	
	71	Irpinia, Italy-01	Arienzo	6.9	53	11.2	
	72	El Mayor-Cucapah, Mexico	RANCHO SAN LUIS	7.2	45	11.3	
	73	Chi-Chi, Taiwan-04	CHY079	6.2	50	11.4	
	74	Joshua Tree, CA	Morongo Valley Fire Station	6.1	22	11.4	
	75	Duzce, Turkey	Mudurnu	7.1	34	11.5	
	76	Irpinia, Italy-01	Rionero In Vulture	6.9	30	11.5	
	77	Chi-Chi, Taiwan-04	CHY042	6.2	34	11.6	
8	78	L'Aquila, Italy	Sulmona	6.3	39	12	**12.8**
	79	Morgan Hill	Corralitos	6.2	23	12	
	80	Landers	Whitewater Trout Farm	7.3	27	12.3	
	81	Umbria Marche, Italy	Matelica	6.0	25	12.6	
	82	Irpinia, Italy-01	Torre Del Greco	6.9	60	12.6	
	83	Landers	Silent Valley – Poppet Flat	7.3	51	13	
	84	Parkfield-02, CA	Templeton Hospıtal Grnds.	6.0	43	13.1	
	85	El Mayor-Cucapah, Mexico	Santa Isabel Vıejo	7.2	57	13.1	
	86	Kozani, Greece-01	Kastoria	6.4	50	13.1	
	87	Darfield, New Zealand	Heathcote Valley Primary Sch.	7.0	24	13.4	
	88	Denali, Alaska	Carlo (temp)	7.9	51	13.5	
9	89	Big Bear-01	Highland Fire Station	6.5	26	13.5	**14.2**
	90	Landers	Big Bear Lake – Civic Center	7.3	45	13.6	
	91	Darfield, New Zealand	RPZ	7.0	58	13.9	
	92	Tottori, Japan	SMNH11	6.6	40	14	
	93	Tottori, Japan	OKYH05	6.6	47	14.1	

Table 4.2. *(Continued)*

Gr.no	No	Event	Station	M_W	R (km)	A_p/V_p (s^{-1})	Avg. A_p/V_p (s^{-1})
	94	Chalfant Valley-02	Convict Creek	6.2	31	14.2	
	95	L'Aquila, Italy	Leonessa	6.3	36	14.4	
	96	Griva, Greece	Kilkis	6.1	29	14.4	
	97	Big Bear-01	Rancho Cucamonga – Deer Can	6.5	60	14.8	
	98	Irpinia, Italy-01	Mercato San Severino	6.9	30	14.8	
	99	Chalfant Valley-02	Benton	6.2	22	15	
10	100	Irpinia, Italy-02	Mercato San Severino	6.2	44	15.4	**27.2**
	101	Chi-Chi, Taiwan-04	CHY102	6.2	39	15.5	
	102	San Fernando	Pasadena – Old Seismo Lab	6.6	22	16.2	
	103	Iwate, Japan	AKTH05	6.9	39	16.8	
	104	Whittier Narrows-01	LA – Wonderland Ave	6.0	28	25	
	105	Whittier Narrows-01	Vasquez Rocks Park	6.0	50	27.3	
	106	Sierra Madre	Vasquez Rocks Park	5.6	40	32.3	
	107	Iwate, Japan	MYGH03	6.9	57	32.5	
	108	Molise-02, Italy	Sannicandro	5.7	51	34.9	
	109	Iwate, Japan	MYGH04	6.9	40	41.2	
	110	Iwate, Japan	MYGH11	6.9	57	42.2	

Table 4.3. *Selected NFGM Records*

Gr.No	No	Event	Station	M_W	T_p (s)	Avg. T_p (s)
1	1	Coalinga-07	Coalinga-14th & Elm (Old CHP)	5.2	0.399	**0.70**
	2	Northridge-01	Pacoima Dam (downstr)	6.7	0.504	
	3	Coalinga-05	Oil City	5.8	0.693	
	4	Yountville	Napa Fire Station #3	5.0	0.728	
	5	San Salvador	Geotech Investig Center	5.8	0.861	
	6	Morgan Hill	Coyote Lake Dam (SW Abut)	6.2	0.952	
	7	Whittier Narrows-01	Downey - Co Maint Bldg	6.0	0.791	
2	8	N. Palm Springs	North Palm Springs	6.1	1.379	**1.45**
	9	Morgan Hill	Gilroy Array #6	6.2	1.239	
	10	Chi-Chi, Taiwan-03	CHY080	6.2	1.351	
	11	San Fernando	Pacoima Dam (upper left abut)	6.6	1.596	
	12	Kobe, Japan	Takarazuka	6.9	1.428	
	13	Taiwan SMART1(40)	SMART1 M07	6.3	1.554	
	14	Taiwan SMART1(40)	SMART1 C00	6.3	1.568	

Table 4.3. *(Continued)*

Gr.No	No	Event	Station	M_W	T_P (s)	Avg. T_P (s)
3	15	Kobe, Japan	Takatori	6.9	1.624	**2.01**
	16	Northridge-01	LA Dam	6.7	1.652	
	17	Chi-Chi, Taiwan	CHY035	7.6	1.435	
	18	Superstition Hills-02	Parachute Test Site	6.5	2.282	
	19	Imperial Valley-06	Agrarias	6.5	2.296	
	20	Northridge-01	Newhall - W Pico Canyon Rd.	6.7	2.408	
	21	Northridge-01	LA - Wadsworth VA Hospital North	6.7	2.359	
4	22	Chi-Chi, Taiwan-03	CHY024	6.2	3.185	**3.42**
	23	Chi-Chi, Taiwan	TAP003	7.6	3.409	
	24	Northridge-01	Sylmar - Converter Sta	6.7	3.479	
	25	Imperial Valley-06	EC Meloland Overpass FF	6.5	3.346	
	26	Northridge-01	Sylmar - Converter Sta East	6.7	3.486	
	27	Northridge-01	Jensen Filter Plant	6.7	3.528	
	28	Northridge-01	Jensen Filter Plant Generator	6.7	3.528	
5	29	Westmorland	Parachute Test Site	5.9	3.577	**4.02**
	30	Imperial Valley-06	Brawley Airport	6.5	4.025	
	31	Imperial Valley-06	El Centro Array #6	6.5	3.836	
	32	Chi-Chi, Taiwan	TCU076	7.6	3.983	
	33	Imperial Valley-06	El Centro Array #5	6.5	4.046	
	34	Loma Prieta	Saratoga - Aloha Ave	6.9	4.473	
	35	Imperial Valley-06	El Centro Array #7	6.5	4.228	
6	36	Landers	Yermo Fire Station	7.3	7.504	**6.14**
	37	Imperial Valley-06	El Centro Differential Array	6.5	5.859	
	38	Imperial Valley-06	El Centro Array #8	6.5	5.39	
	39	Chi-Chi, Taiwan	TCU029	7.6	6.447	
	40	Kocaeli, Turkey	Gebze	7.5	5.873	
	41	Chi-Chi, Taiwan	TCU031	7.6	6.188	
	42	Chi-Chi, Taiwan	TCU065	7.6	5.74	
7	43	Imperial Valley-06	El Centro Array #11	6.5	7.364	**8.67**
	44	Landers	Barstow	7.3	8.932	
	45	Chi-Chi, Taiwan	TCU087	7.6	9.044	
	46	Chi-Chi, Taiwan	TCU128	7.6	9.009	
	47	Chi-Chi, Taiwan	TCU046	7.6	8.582	
	48	Chi-Chi, Taiwan	TCU034	7.6	8.61	
	49	Chi-Chi, Taiwan	TCU042	7.6	9.107	

CHAPTER 5

DEVELOPMENT OF THE EQUATIONS TO OBTAIN MAXIMUM AND RESIDUAL ISOLATOR DISPLACEMENTS

5.1. Introduction

In this section, residual and maximum displacement equations are derived for seismic isolated systems subjected to FFGM and NFGM. For this purpose, the NLTHA of the SDOF seismic isolated structures are performed for the FFGM and NFGM and range of parameters considered in this research study. The averages of the isolator displacements are obtained for each group of ground motions, which are classified according to their A_p/V_p for FFGM and T_p for NFGM. Next, the variations of the residual and maximum displacements are plotted as functions of the various combinations of the parameters considered in the analyses. Then, nonlinear regression analyses (via Microsoft Excel) are performed to formulate the residual and maximum displacements as functions of these parameters. This resulted in four different equations for residual and maximum displacements, that is, two equations for FFGM and two equations for NFGM.

5.2. Variation of Displacement Equations as a Function of Various Parameters

In this section, the variations of the residual and maximum displacements as functions of the parameters considered in this research study are investigated to determine the form of the proposed maximum and residual displacement equations. The parameters used to plot the variation of the residual and maximum displacements are; mA_p, Q_d, T_d and A_p/V_p for FFGM and mA_p, Q_d, T_d and T_p for NFGM. The variation of the maximum and residual displacements as functions of the above-mentioned parameters is plotted respectively in Figure 5.1 and Figure 5.2 for FFGM and in Figure 5.3 and Figure 5.4 for NFGM. It is noteworthy that in some of the figures, the trends of the least square fits are not seen clearly since most of the data points are concentrated at the lower parts of the plots. The vertical axis for these plots could be scaled to examine the trend of the trendlines better, however this is not preferred since general dispersion of the data points would not be observed clearly if a scale is applied. In the figures, the nonlinear minimum least square fit of the data points using a power function of the form, $Y=aX^b$ is plotted with a solid line. It is observed that for both FFGM and NFGM, the maximum displacement increases with increasing values of mA_p and T_d, but decreases, with increasing values of Q_d and A_p/V_p for FFGM. For NFGM, the observations are similar except for T_p, where the maximum displacement increases with increasing T_p. This is expected since seismic isolation systems with lower characteristic strength, Q_d, smaller restoring force capability (or large post-elastic period, T_d) subjected to low frequency (small A_p/V_p) FFGM or NFGM with large pulse period, T_p having larger intensity (mA_p) tend to have larger isolator displacements. It is noteworthy that FFGM with large A_p/V_p ratio contain high frequency acceleration pulses that load and unload the structure in very short time intervals. Therefore, once the isolation system yields or slides, the post-yield displacement is kept for a very short time interval as the A_p/V_p ratio of the FFGM increases resulting in smaller isolator displacements. On the other hand, in the case of seismic isolation systems subjected to NFGM with large pulse period, once the isolation system yields, the post-yield displacement is kept for an extended period of time resulting in larger isolator displacements.

For the residual displacement, Figure 5.2 and Figure 5.4 reveal that for both FFGM and NFGM, the residual displacement increases with increasing values of mA_p, Q_d and T_d, but decreases, with increasing values A_p/V_p for FFGM. For NFGM, the observations are similar except for T_p, where the residual displacement increases with increasing T_p. This is expected since seismic isolation systems with larger characteristic strength, Q_d, smaller restoring force capability (or large post-elastic period, T_d) subjected to low frequency (small A_p/V_p) FFGM or NFGM with large pulse period, T_p having larger intensity (mA_p) tend to have larger residual displacements.

This may also be explained by considering the force (F) displacement (d) relationship of a typical isolator where $F=Q_d + k_d d$. At the end of the earthquake, the isolator force is equal to zero. Thus, setting F=0 and solving for d, the residual displacement is obtained as: $d_{res}= -Q_d/k_d$. The derived equation clearly shows that the residual displacement increases for isolators with larger Q_d and smaller k_d (or larger T_d).

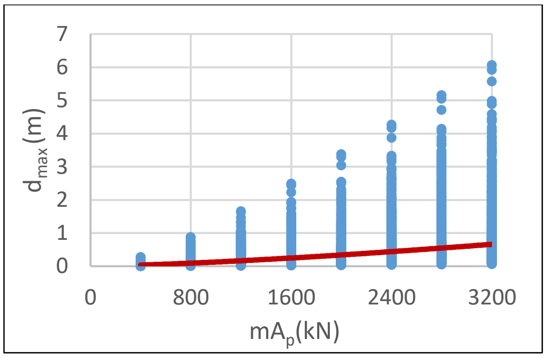

(a)

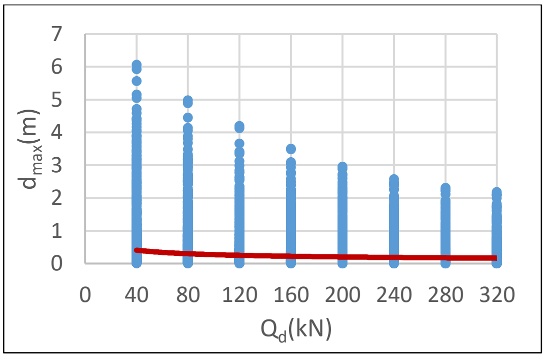

(b)

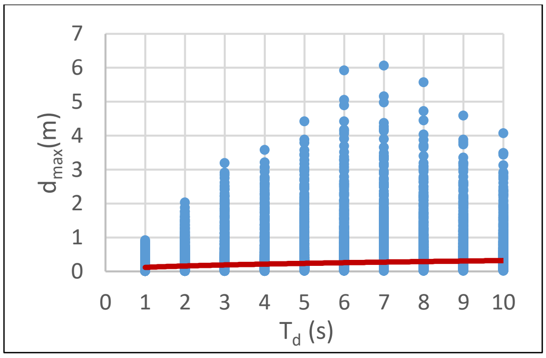

(c)

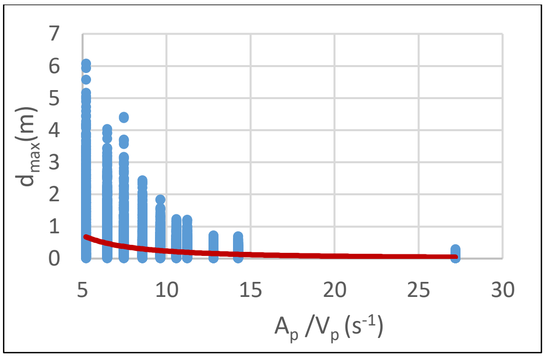

(d)

Figure 5.1. Variation of the maximum displacements for FFGM with (a) mA_p, (b) Q_d, (c) T_d, (d) A_p/V_p

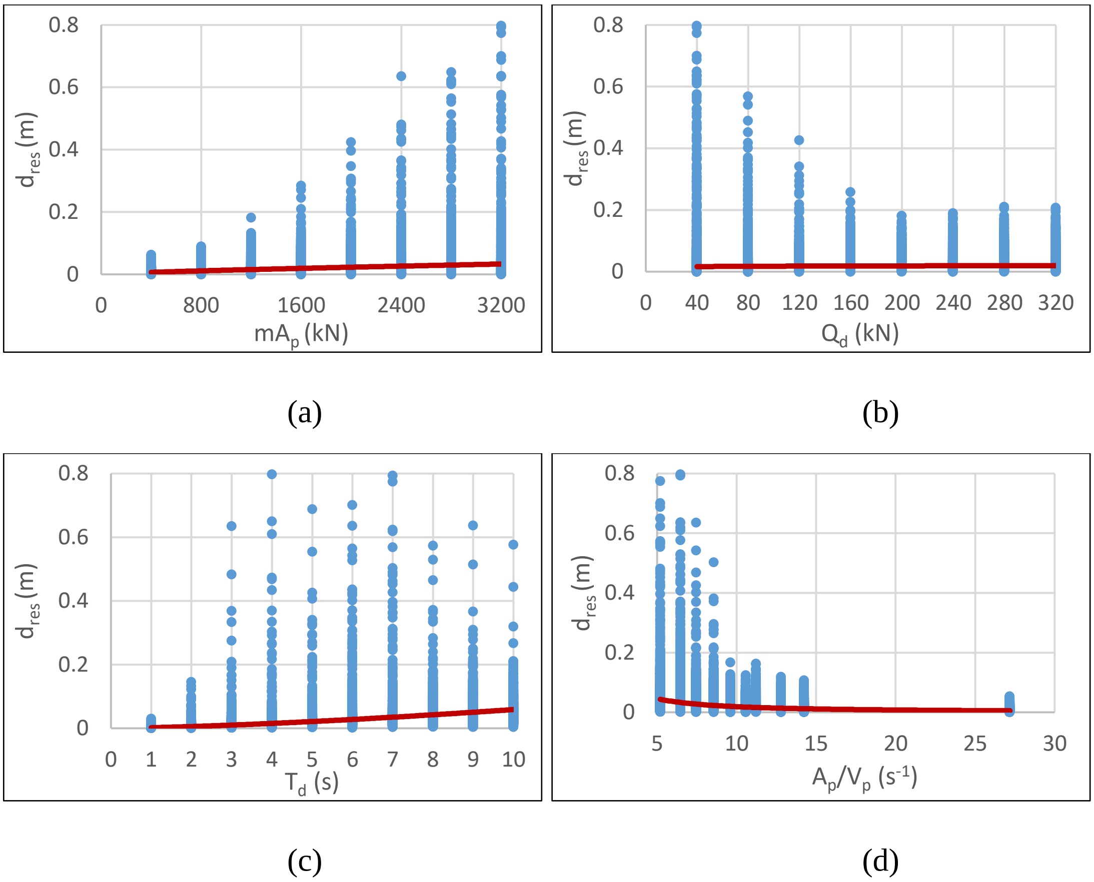

Figure 5.2. Variation of the residual displacements for FFGM with (a) mA_p, (b) Q_d, (c) T_d, (d) A_p/V_p

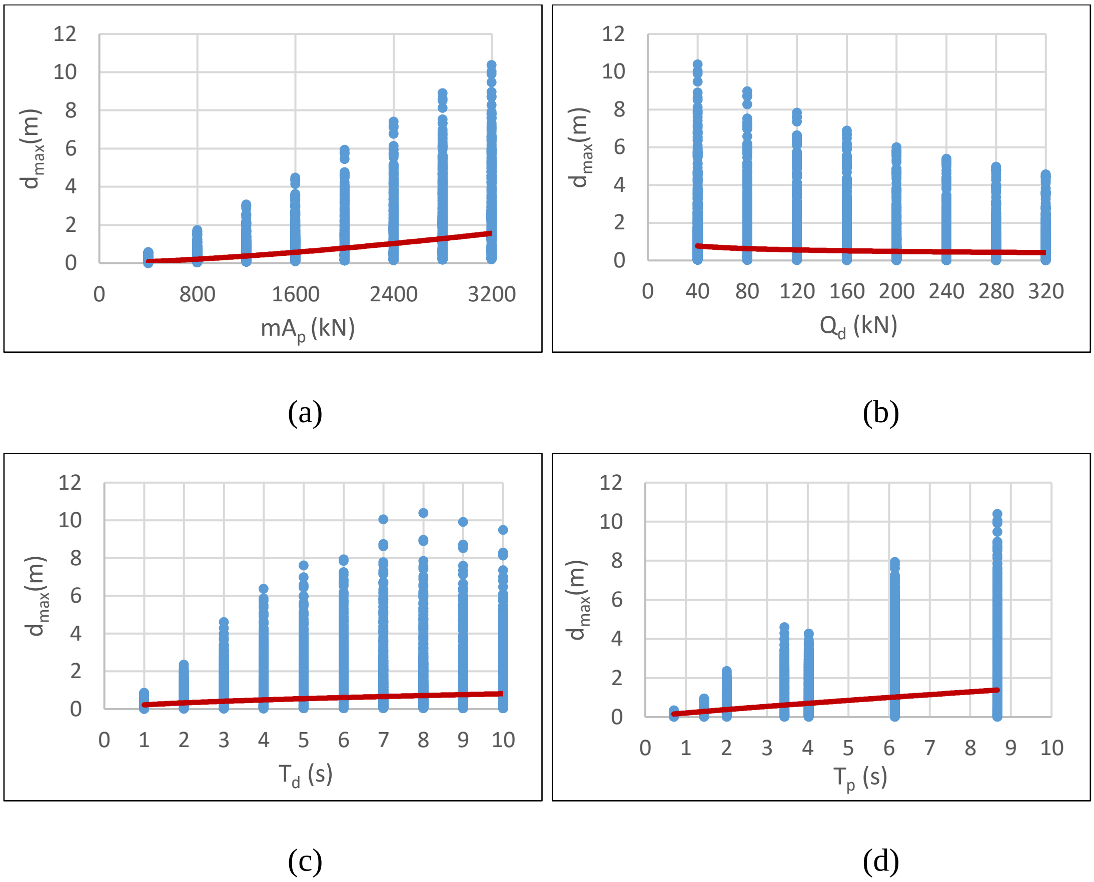

Figure 5.3. Variation of the maximum displacements for NFGM with (a) mA_p, (b) Q_d, (c) T_d, (d) T_p

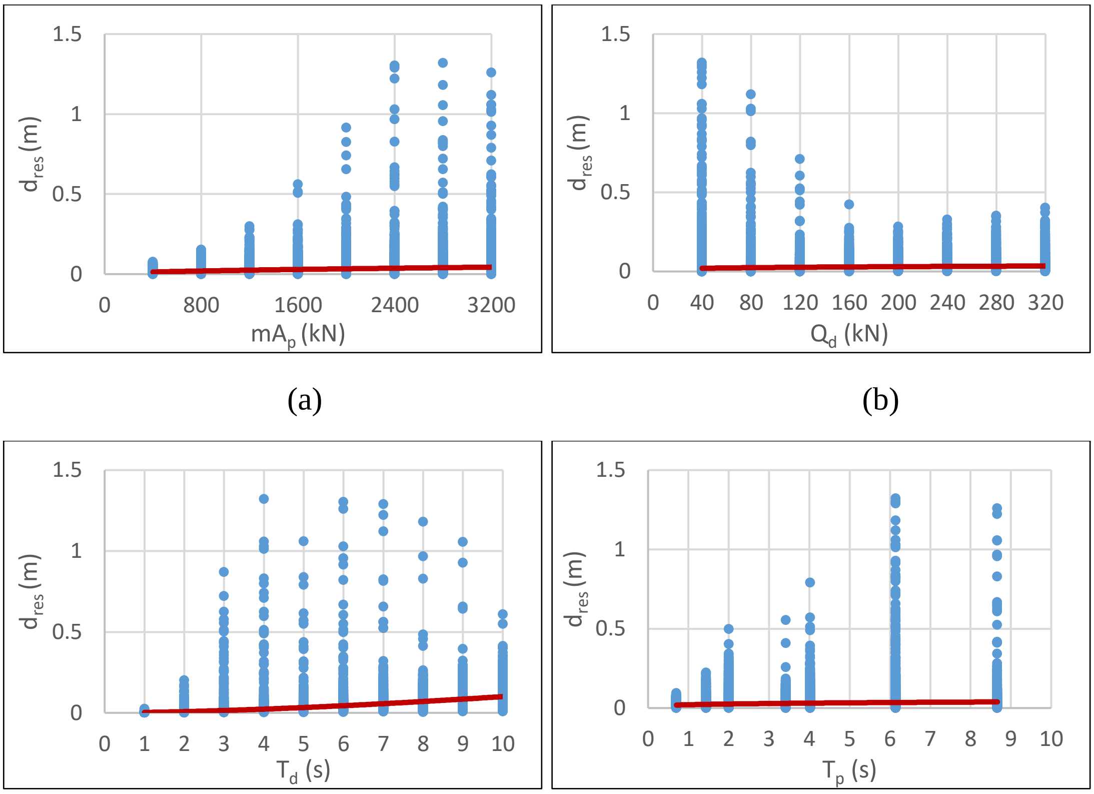

(a) (b) (c) (d)

Figure 5.4. Variation of the residual displacements for NFGM with (a) mA_p, (b) Q_d, (c) T_d, (d) T_p

5.3. Development of the Proposed Residual and Maximum Displacement Equations

To obtain the maximum and residual displacement equations, first the nonlinear minimum least square fits of the data points in Figure 5.5 to Figure 5.8 are obtained in Microsoft Excel software considering five different functions, namely; linear, power, polynomial, logarithmic and exponential. Among all the functions in the software, the power function of the form $Y=aX^b$ yields the largest coefficient of determination, R^2 in the nonlinear regression analyses of the plots compared to other functional forms. Since larger R^2 indicate a better fit, the maximum and residual displacement equations are assumed to have the following form for FFGM;

$$d_{max}\ or\ d_{res} = a\left(mA_p\right)^{b1} Q_d{}^{b2}\, T_d{}^{b3} \left(\frac{A_p}{V_p}\right)^{b4} \tag{6}$$

For NFGM, the equation is similar except the term A_p/V_p in the above equation is replaced by T_p. The procedure below is followed to obtain the constants *a, b1, b2, b3* and *b4* in the above equation for maximum displacement considering the data for FFGM. First, the maximum displacement data, d_{max}, is plotted as a function of the first parameter, mA_p and a nonlinear minimum least square fit of the data in the form of a power function, $F1=a_1(mA_p)^{b1}$ is obtained (Figure 5.5(a)). Next, the maximum displacement, d_{max} is divided by *F1,* to decouple the data points from the effect of the term mA_p and the decoupled data ($d_{max}/F1$) is plotted as a function of Q_d. Then, a new function of the form $F2=a_2(Q_d)^{b2}$ is obtained (Figure 5.5(b)). Afterward, the maximum displacement, d_{max} is divided by $F1\times F2$ to decouple the data points from the effect of the terms mA_p and Q_d and the decoupled data $d_{max}/(F1\times F2)$ is plotted as a function of T_d. Subsequently a new function of the form $F3=a_3(T_d)^{b3}$ is obtained (Figure 5.5(c)). Finally, the maximum displacement, d_{max} is divided by $F1\times F2\times F3$ to decouple the data points from the effect of the terms mA_p, Q_d and T_d. Then, the decoupled data d_{max} / $(F1\times F2\times F2)$ is plotted as a function of A_p/V_p. Next, a new function of the form $F4=a_4(A_p/V_p)^{b4}$ is obtained (Figure 5.5 (d)). Since $F4=d_{max}/(F1\times F2\times F3)$ and solving for d_{max}, the equation for the maximum isolator displacement is obtained as; $d_{max} = F1\times F2\times F3\times F4$. Accordingly, the coefficient "*a* "in Eq.6 is obtained as $a= a_1\times a_2\times a_3\times a_4$. A similar procedure is followed to obtain the residual displacement equation for FFGM and both maximum and residual displacement equations for NFGM. Thus, the equations for the maximum and residual displacements for FFGM are as follows;

$$d_{max} = 1.440\left(mA_p\right)^{1.42} Q_d{}^{-0.44}\, T_d{}^{0.43} \left(\frac{A_p}{V_p}\right)^{-1.62} \tag{7}$$

$$d_{res} = 0.085\left(mA_p\right)^{0.78} Q_d{}^{0.08}\, T_d{}^{1.47} \left(\frac{A_p}{V_p}\right)^{-1.28} \tag{8}$$

Similarly, the equations for the maximum and residual displacements for NFGM are obtained as follows;

$$d_{max} = 0.0093(mA_p)^{1.46}\, Q_d{}^{-0.30}\, T_d{}^{0.56}\, T_p{}^{0.88} \tag{9}$$

$$d_{res} = 0.0072(mA_p)^{0.58}\, Q_d{}^{0.26}\, T_d{}^{1.61}\, T_p{}^{0.29} \tag{10}$$

For the equations above, displacements are in mm, force units are kN and the periods are in second.

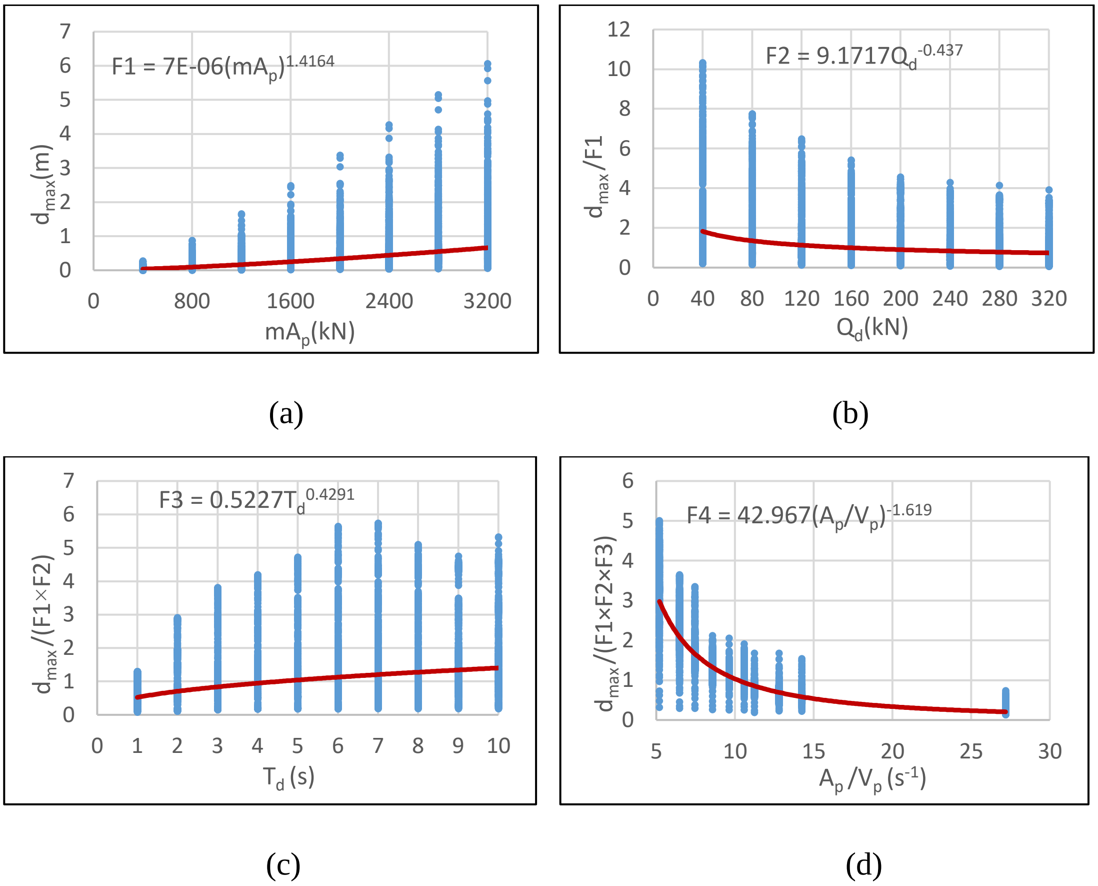

Figure 5.5. Charts to obtain the main formula for maximum displacement for FFGM

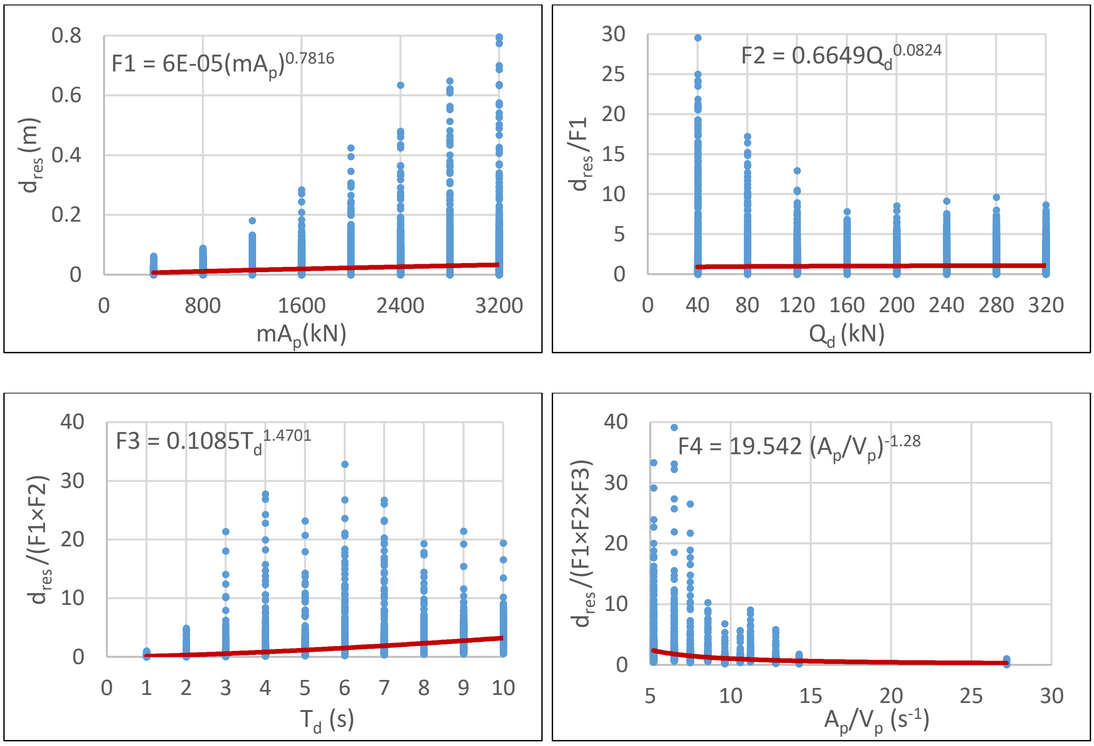

Figure 5.6. Charts to obtain the main formula for residual displacement for FFGM

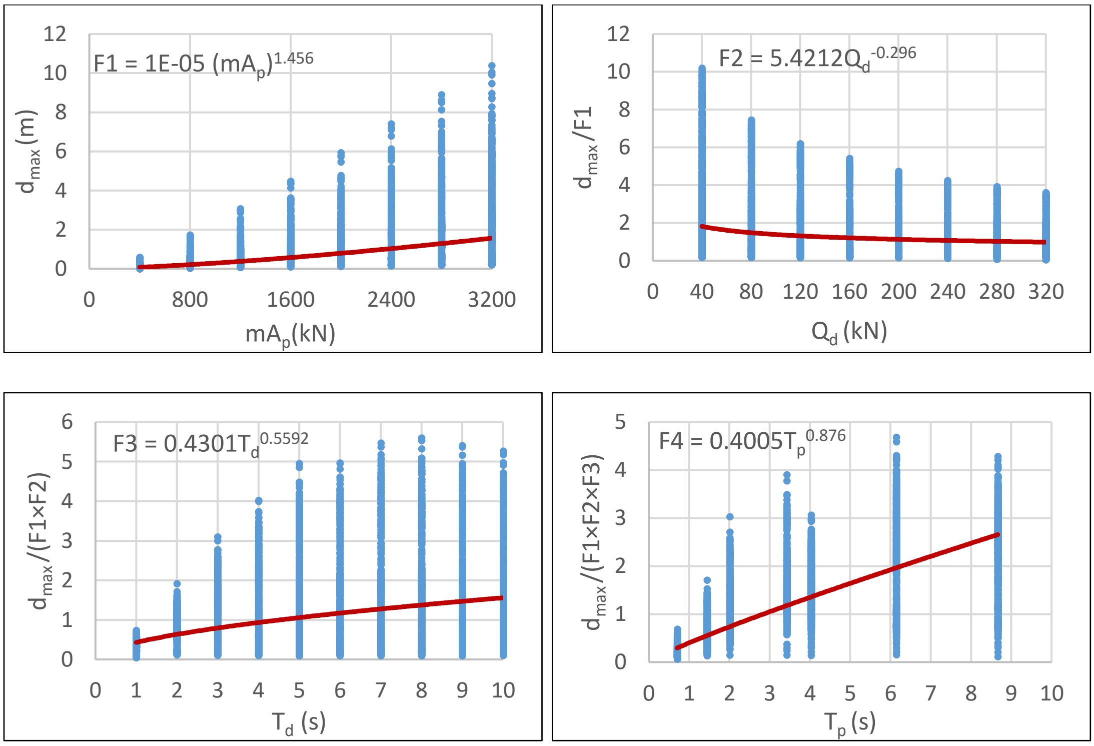

Figure 5.7. Charts to obtain the main formula for maximum displacement for NFGM

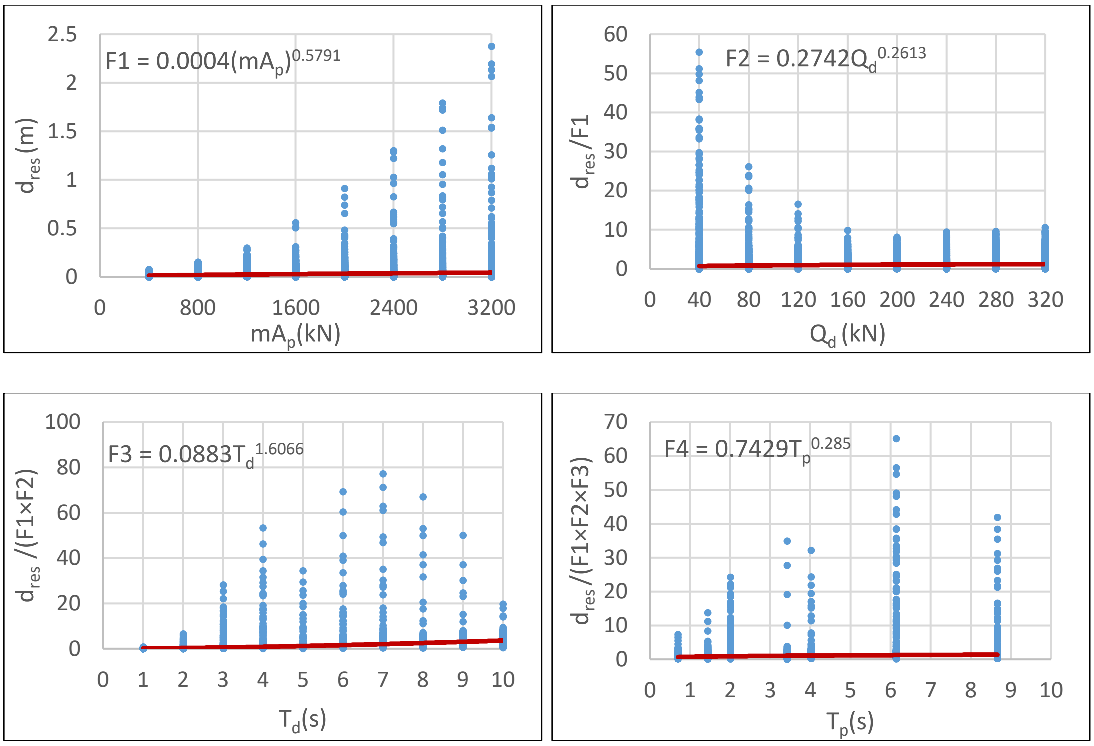

Figure 5.8. Charts to obtain the main formula for residual displacement for NFGM

CHAPTER 6

DEVELOPMENT OF RESTORING FORCE EQUATIONS TO LIMIT MAXIMUM AND RESIDUAL DISPLACEMENTS

6.1. Formulation of Restoring Force Equations

In this section, restoring force equations are developed for seismic isolated structures subjected to FFGM and NFGM. The developed equations are based on limiting the post-elastic period of seismic isolated structures subjected to FFGM and NFGM to ensure reasonable levels of residual and maximum isolator displacements. Accordingly, four equations are developed; two equations to limit the residual and maximum displacements of seismic isolated structures subjected to FFGM and in a similar way, two equations for seismic isolated structures subjected to NFGM.

Residual displacement is generally expressed as a fraction of the maximum displacement [8], [10]. Accordingly, to obtain the upper limit of the post-elastic period to ensure reasonable levels of residual displacements of seismic isolated structures subjected to FFGM, first the residual displacement equation for FFGM (Eq.8) is divided by the corresponding maximum displacement equation (Eq.7) to obtain the d_{res}/d_{max} ratio as follows;

$$\frac{d_{res}}{d_{max}} = 0.059\left(mA_p\right)^{-0.64} {Q_d}^{0.52}\, {T_d}^{1.04}\left(\frac{A_p}{V_p}\right)^{0.34} \tag{11}$$

Solving for T_d from Eq.11 and knowing that for a desired level of d_{res}/d_{max} ratio, T_d should be smaller than a certain threshold value, the following equation is obtained;

$$T_d < \frac{15.2(mA_p)^{0.62}\left(\frac{d_{res}}{d_{max}}\right)^{0.96}}{{Q_d}^{0.50}\left(\frac{A_p}{V_p}\right)^{0.33}} \tag{12}$$

To determine the threshold value of d_{res}/d_{max} , the parameters which magnify and reduce the d_{res}/d_{max} ratio are grouped and their ratio, κ_{FF} is calculated as follows;

$$\kappa_{\mathrm{FF}} = \frac{(mA_p)^{0.64}}{Q_d^{\,0.52}\, T_d^{\,1.04} \left(\frac{A_p}{V_p}\right)^{0.34}} \tag{13}$$

Next, the d_{res}/d_{max} ratio is plotted as a function of κ_{FF} in Figure 6.1(a) for all the range of parameters considered in the analyses and a power function is fitted to the data points by a minimum least square curve fitting procedure. As observed from the figure, at a certain threshold value on the horizontal axis, this power function starts to become asymptotic to the vertical axis, which represent the d_{res}/d_{max} ratio. This threshold value corresponds to approximately d_{res}/d_{max} =0.10. By substituting d_{res}/d_{max}=0.10 in Eq.12 the maximum value of T_d, (minimum restoring force requirement) to limit the residual displacement is obtained as follows;

$$T_d < \frac{1.67(mA_p)^{0.62}}{Q_d^{\,0.50} \left(\frac{A_p}{V_p}\right)^{0.33}} \tag{14}$$

In some design applications, a residual displacement smaller than the recommended value of d_{res}/d_{max}=0.10 may be desired to ensure the serviceability of the seismic isolated structure after a potential earthquake. In such a case the desired value of d_{res}/d_{max} ratio (e.g. 0.05) may be substituted in Eq.12 to obtain the maximum value of T_d, to limit the residual displacement to the desired level.

A similar procedure is followed to determine the limiting value of T_d, to ensure reasonable levels of maximum isolator displacements of seismic isolated structurers subjected to FFGM. For this purpose, first, T_d is solved from Eq. 7 and knowing that for a desired level of d_{max}, T_d should be smaller than a certain threshold value, the following equation is obtained;

$$T_d < \frac{0.43 Q_d^{\,1.02}\, (d_{max})^{2.33} \left(\frac{A_p}{V_p}\right)^{3.77}}{(mA_p)^{3.30}} \tag{15}$$

To determine the threshold value of d_{max}, the parameters which magnify and reduce the maximum displacement (Eq.7) are grouped and their ratio, η_{FF} is calculated as follows;

$$\eta_{\mathrm{FF}} = \frac{\left(\frac{A_p}{V_p}\right)^{1.62} {Q_d}^{0.44}}{\left(mA_p\right)^{1.42} {T_d}^{0.43}} \tag{16}$$

Next, d_{max} is plotted as a function η_{FF} in Figure 6.1(b) for all the range of parameters considered in the analyses and a power function is fitted to the data points by a minimum least square curve fitting procedure. As observed from the figure, at a certain threshold value on the horizontal axis, this power function starts to become asymptotic to the vertical axis, which represent the d_{max}. A feasible value of maximum isolation system displacement is considered as d_{max}= 600 mm. By substituting d_{max}=600 mm in Eq.15 the maximum value of T_d, (minimum restoring force requirement) to limit the maximum displacement is obtained as follows;

$$T_d < \frac{1272 \times 10^3 \left(\frac{A_p}{V_p}\right)^{3.77} {Q_d}^{1.02}}{(mA_p)^{3.30}} \tag{17}$$

However, imposing a limit on the maximum displacement by limiting the post-elastic period, T_d, may result in large base shears. Therefore, in such cases, a desired displacement level (larger than 600 mm) corresponding to a desired level of base shear may be substituted in Eq. 15 to obtain the limiting value of T_d.

A similar procedure is followed to obtain the maximum value of T_d, to limit the residual (Eq.18) and maximum (Eq.19) isolation system displacements of seismic isolated structures subjected to NFGM as follows;

$$T_d < \frac{1.28(mA_p)^{0.84} \; {T_p}^{0.56} \left(\frac{d_{res}}{d_{max}}\right)^{0.95}}{{Q_d}^{0.53}} \tag{18}$$

$$T_d < \frac{4240 {Q_d}^{0.54} \, (d_{max})^{1.79}}{(mA_p)^{2.61} \, {T_p}^{1.57}} \tag{19}$$

Next, a procedure similar to that of FFGM is followed to determine the threshold values of d_{res}/d_{max} and d_{max}. Accordingly, first the d_{res}/d_{max} vs. κ_{NF} and d_{max} vs η_{NF} plots shown in Figure 6.2 are obtained. From the plot, the threshold values of d_{res}/d_{max} and d_{max} are determined as 0.1 and 600 mm respectively. These values are then substituted in Eqs.18 and 19 to obtain the following equations to calculate the maximum value of T_d for limiting the residual (Eq.20) and maximum (Eq.21) displacements for NFGM as follows;

$$T_d < \frac{0.144 (mA_p)^{0.84} \, {T_p}^{0.56}}{{Q_d}^{0.53}} \tag{20}$$

$$T_d < \frac{3.98 \times 10^8 \, {Q_d}^{0.54}}{(mA_p)^{2.61} \, {T_p}^{1.57}} \tag{21}$$

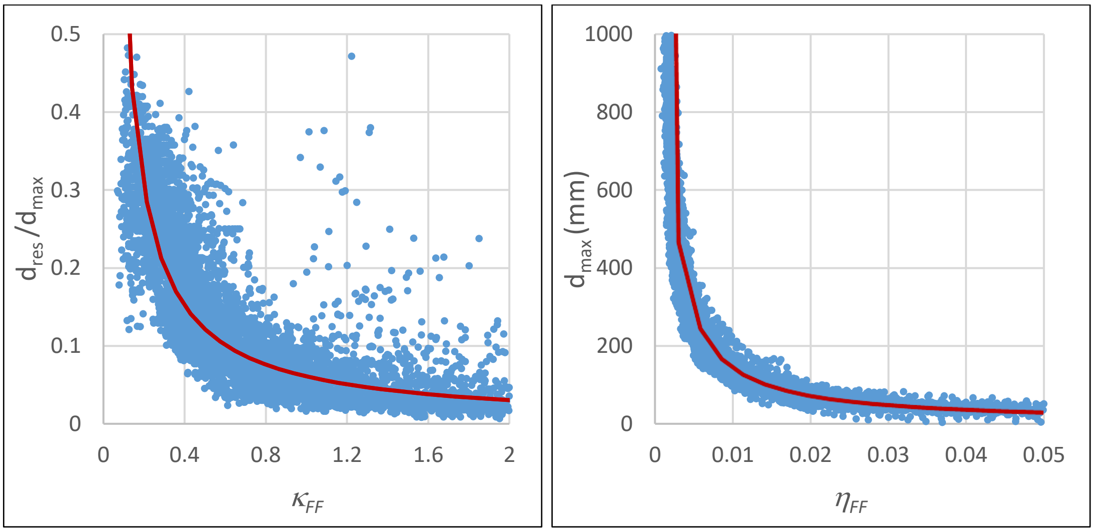

(a) (b)

Figure 6.1. Plots for d_{res}/d_{max} and d_{max} for FFGM

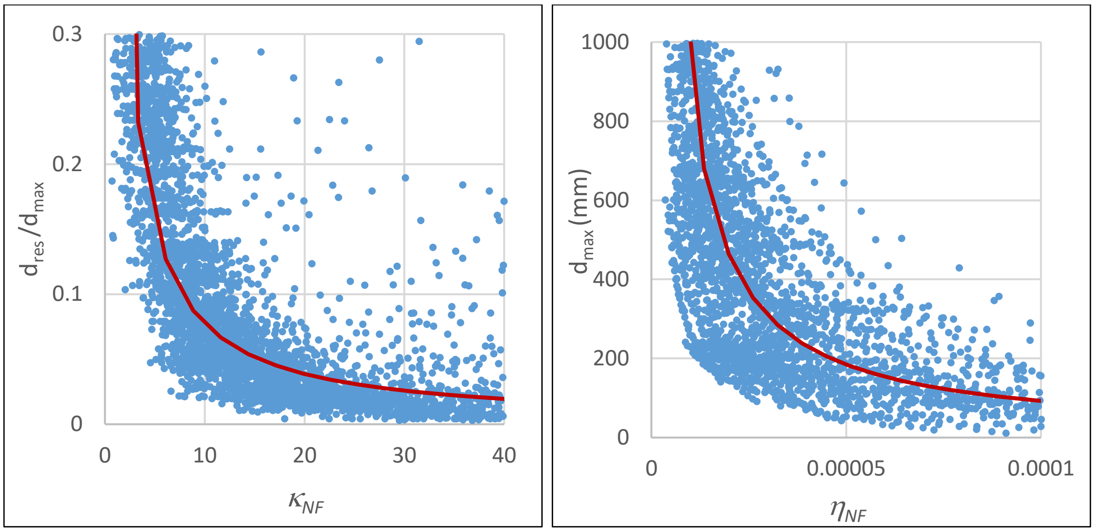

(a) (b)

Figure 6.2. Plots for d_{res}/d_{max} and d_{max} for NFGM

6.2. A_p/V_p-T_c and T_p-T_c Relationships for FFGM and NFGM

The developed restoring force equations contain the parameters A_p/V_p and T_p. However, using the parameters A_p/V_p and T_p in these equations is not practical since only the design spectrum is available to the designer. Therefore, relationships between the second corner period, T_c of the design spectrum and A_p/V_p for FFGM as well as T_c and T_p for NFGM is needed to replace A_p/V_p and T_p in the restoring force equations by T_c.

To obtain relationships between the corner period, T_c of the design spectrum and A_p/V_p for FFGM as well as T_c and T_p for NFGM, the response spectra of the groups of ground motion considered in this research study (Table 4.2 and Table 4.3) are used. First, the response spectra of the ground motions within each group are scaled to have identical peak ground accelerations and the average response spectrum for each group of ground motions is obtained. Then a smoothed spectrum is fitted to the average response spectrum for each group of ground motions. The smoothed response spectrum is composed of three parts; the ascending or acceleration sensitive region, the flat or velocity sensitive region and the descending or displacement sensitive region. To obtain the smoothed response spectra, the steps below are followed;

i. First, the starting points of the velocity and displacement sensitive regions are identified by a careful examination of the average response spectrum curve. Next, a minimum least square power function is fitted to the plot of the spectral acceleration (S_a) versus period (T) data of the average response spectrum curve between the starting point of the displacement sensitive region and the end point of the spectrum and an equation in the form given below is obtained;

$$S_a = \frac{\beta}{T^{\alpha}} \tag{22}$$

where α and β are coefficients determined by minimum least squares regression analyses.

ii. Then, the spectral amplitude of the flat or velocity sensitive region of the response spectrum curve is identified by taking the weighted average of the spectral accelerations between the starting points of the velocity and displacement sensitive regions using the following equation;

$$S_a = \frac{\sum S_{ai} \Delta T_i}{\sum \Delta T_i} \tag{23}$$

where S_{ai} is the spectral acceleration of the data point i and ΔT_i is the tributary time period of the data point under consideration.

iii. Finally, the ascending or acceleration sensitive region of the smoothed response spectrum curve is defined by fitting a minimum least square linear function within the region as follows,

$$S_a = A_p + \lambda T \tag{24}$$

where λ is the slope of this linear function. The intersection points of Eq.23 and Eq.24 defines the first corner period while the intersection point of Eq.22 and Eq.23 defines the second corner period (T_c) of the smoothed response spectrum curve.

The response spectra of the FFGM and NFGM within each group together with their average and smoothed response spectra are plotted in Figure 6.3 and Figure 6.4. The numbers in the legends are associated with the ground motions listed in Table 4.2 for FFGM and Table 4.3 for NFGM. The average A_p/V_p ratios of the groups of FFGM versus the corner periods, T_c, of their spectra is plotted in Figure 6.5 (a) and a minimum least square power function is fitted to the data points to obtain the following relationship between A_p/V_p and T_c;

$$\frac{A_p}{V_p} = \frac{5}{T_c} \tag{25}$$

Similarly, the average T_p of the groups of NFGM versus the corner periods, T_c, of their spectra is plotted in Figure 6.5 (b) and a minimum least square linear function is fitted to the data points to obtain the following relationship between T_p and T_c;

$$T_p = 1.4T_c \tag{26}$$

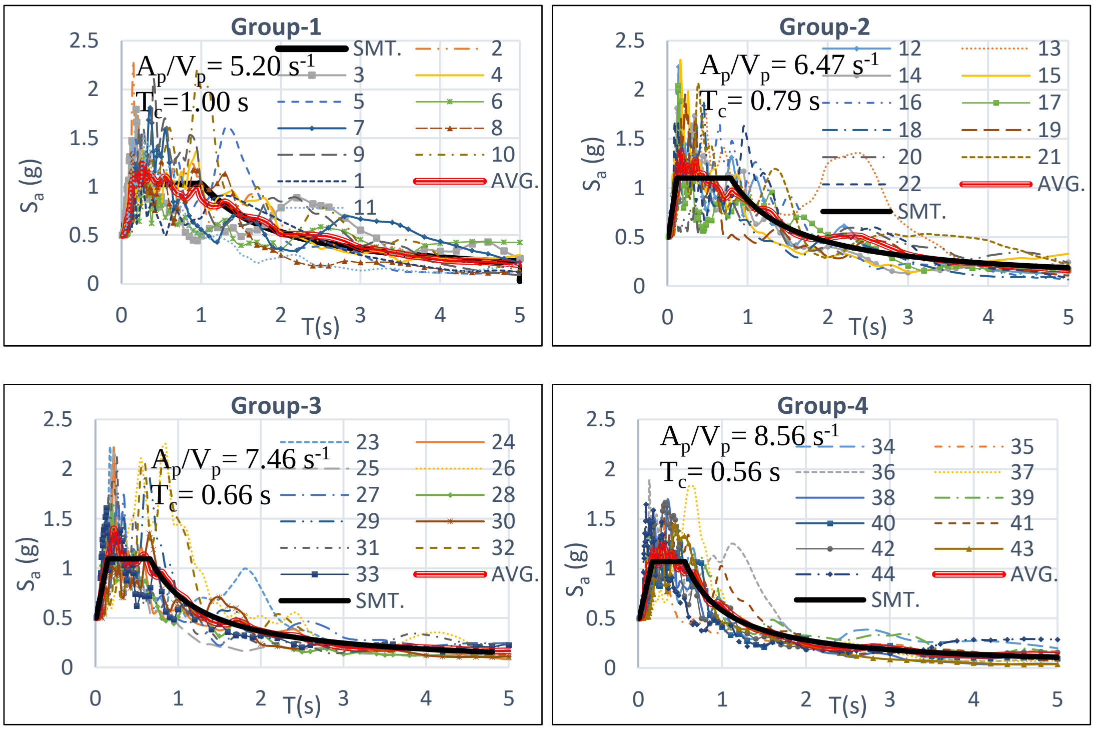

Figure 6.3. Single, average and smoothed response spectra for FFGM. AVG=average, SMT=Smoothed

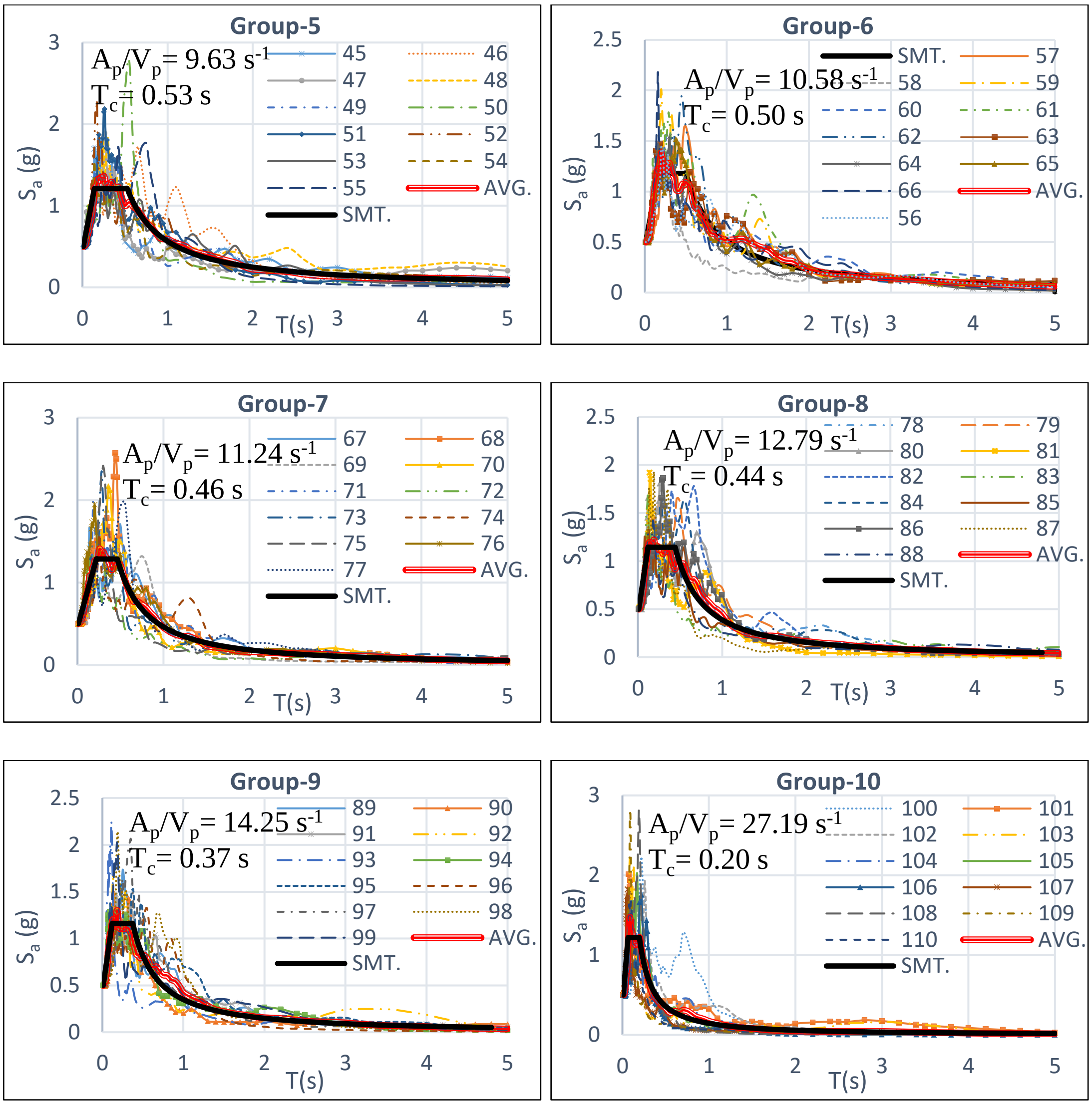

Figure 6.3. (Continued)

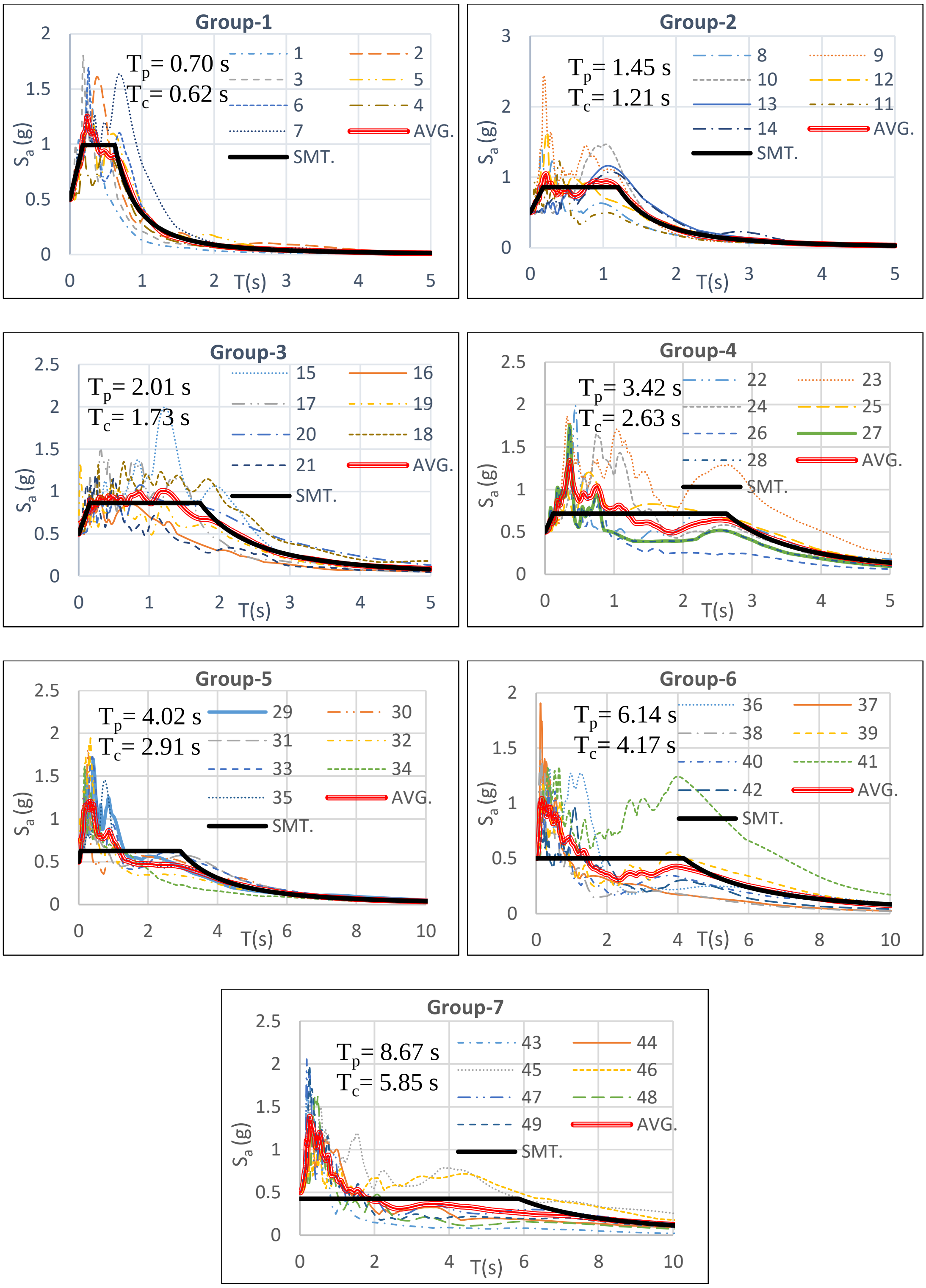

*Figure 6.4.*Single, average and smoothed response spectra for NFGM. AVG=average, SMT=Smoothed

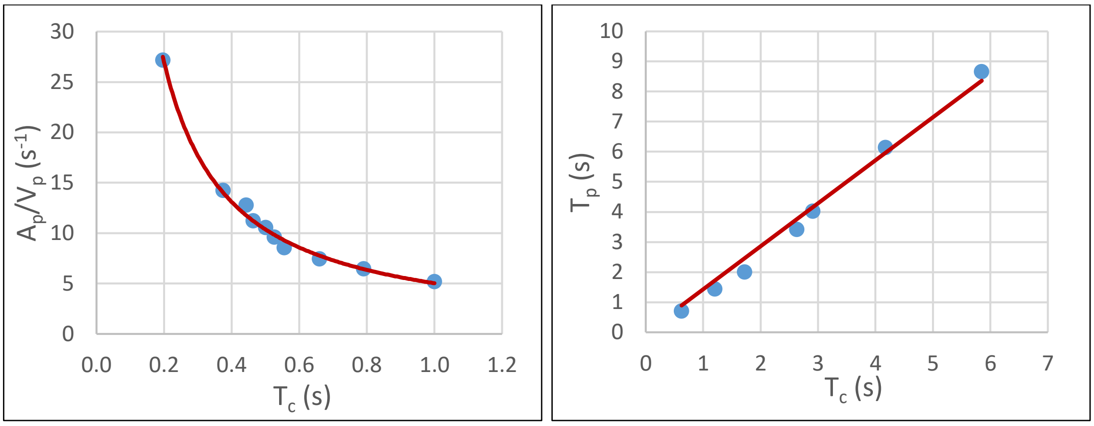

(a) (b)

Figure 6.5. (a) Plot of T_c and average A_p/V_p for FFGM, (b) Plot of T_c and average T_p for NFGM

6.3. Verification of A_p/V_p-T_c and T_p-T_c Relationships

In this section, Eqs.25 and 26, representing the relationships between A_p/V_p and T_c for FFGM as well as T_p and T_c for NFGM are verified. For this purpose, completely different sets of FFGM and NFGM are selected. Properties of these selected ground motions are listed in Table 6.1 and Table 6.2 for FFGM and NFGM respectively. In these tables, there are three groups of seven ground motions. First, the response spectra of the ground motions within each group are scaled to have identical peak ground accelerations and the average response spectrum for the group of ground motions is obtained. Then, these average response spectra are smoothed by using the procedure defined earlier. The smoothed average response spectrum curves for each group are plotted in Figure 6.6(a) and Figure 6.6(b) for FFGM and NFGM respectively. The corner periods for each group of FFGM and NFGM are then determined from the plots in Figure 6.6.

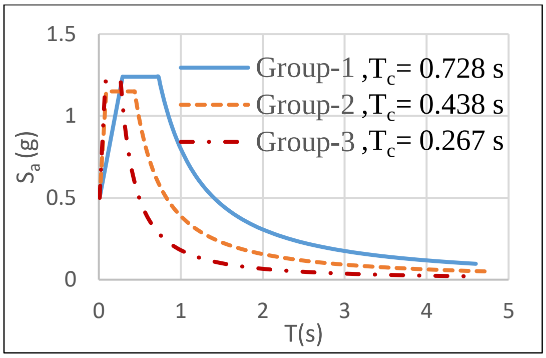

(a)

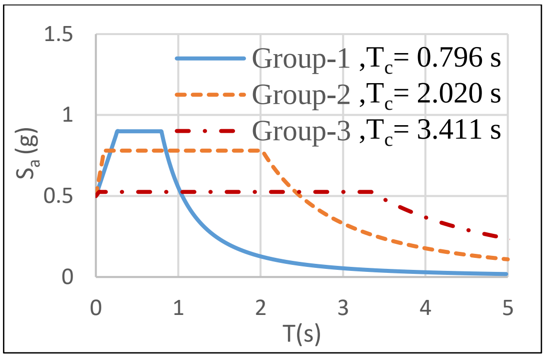

(b)

Figure 6.6. Smoothed average response spectrum curves for each group used for verification of (a) FFGM and (b) NFGM.

The ratios of the T_c values obtained from the smoothed spectra and those calculated using the derived relationships (Eq.25 and 26) are shown in a bar chart form in Figure 6.7. As observed from the figure, the ratios are close to unity indicating a resonably good estimation of T_c as afunction A_p/V_p for FFGM and T_p for NFGM.

Table 6.1. *Selected FFGM for verification*

Gr.no	No	Event	Station	M_W	R (km)	A_p/V_p (s^{-1})	Avg. A_p/V_p (s^{-1})
1	1	Parkfield-02, CA	Coalinga - Fire Station 39	6.0	23	7.47	7.760
	2	Morgan Hill	Hollister City Hall	6.2	31	7.01	
	3	Morgan Hill	San Juan Baut., 24 Polk St	6.2	27	7.48	
	4	Borrego	El Centro Array #9	6.5	57	7.40	
	5	Big Bear-01	San Bernardino - E & Hosp.	6.5	35	8.35	
	6	Imperial Valley-06	Coachella Canal #4	6.5	50	7.85	
	7	Chi-Chi, Taiwan-04	CHY015	6.2	50	8.77	
2	8	Landers	Twentynine Palms	7.3	41	12.23	12.030
	9	Tottori, Japan	HRS007	6.6	58	11.68	
	10	Kozani, Greece-01	Kastoria	6.4	50	12.25	
	11	L'Aquila, Italy	Carsoli 1	6.3	35	11.67	
	12	Griva, Greece	Kilkis	6.1	29	13.26	
	13	Chi-Chi, Taiwan-04	CHY019	6.2	54	11.91	
	14	Irpinia, Italy-01	Arienzo	6.9	53	11.19	
3	15	San Fernando	Pasadena - Old Seismo Lab	6.6	22	15.66	20.430
	16	Chi-Chi, Taiwan-04	CHY102	6.2	39	24.69	
	17	Molise-02, Italy	Sannicandro	5.7	51	25.78	
	18	Whittier Narrows-01	LA - Chalon Rd	6.0	35	17.27	

Table 6.1. *(Continued)*

Gr.no	No	Event	Station	M_W	R (km)	A_p/V_p (s^{-1})	Avg. A_p/V_p (s^{-1})
	19	Morgan Hill	UCSC Lick Observatory	6.2	45	19.24	
	20	Tottori, Japan	OKYH14	6.6	27	23.37	
	21	Kobe, Japan	Chihaya	6.9	50	16.97	

Table 6.2. *Selected NFGM for verification*

Gr.No	No	Event	Station	M_w	T_p (s)	Avg. T_p(s)
	1	Northridge-01	Pacoima Dam (upper left)	6.7	0.896	
	2	Chi-Chi, Taiwan-03	TCU076	6.2	0.910	
	3	Coalinga-05	Transmitter Hill	5.8	0.924	
1	4	Whittier Narrows-01	LB - Orange Ave	6.0	0.952	1.041
	5	Mammoth Lakes-06	Long Valley Dam (Upr L Abut)	5.9	1.050	
	6	Coyote Lake	Gilroy Array #6	5.7	1.211	
	7	Northwest China-03	Jiashi	6.1	1.344	
	8	Cape Mendocino	Petrolia	7.0	2.996	
	9	Imperial Valley-06	Aeropuerto Mexicali	6.5	2.422	
	10	Chi-Chi, Taiwan	CHY006	7.6	2.626	
2	11	Erzican, Turkey	Erzincan	6.7	2.653	2.808
	12	Chi-Chi, Taiwan-06	CHY101	6.3	2.765	
	13	Northridge-01	Sylmar - Olive View Med FF	6.7	3.108	
	14	Irpinia, Italy-01	Sturno	6.9	3.088	
	15	Imperial Valley-06	El Centro Array #10	6.5	4.487	
	16	Imperial Valley-06	EC County Center FF	6.5	4.515	
	17	Imperial Valley-06	El Centro Array #4	6.5	4.613	
3	18	Chi-Chi, Taiwan	CHY101	7.6	4.767	4.776
	19	Imperial Valley-06	Holtville Post Office	6.5	4.802	
	20	Landers	Lucerne	7.3	5.103	
	21	Chi-Chi, Taiwan	TCU075	7.6	5.145	

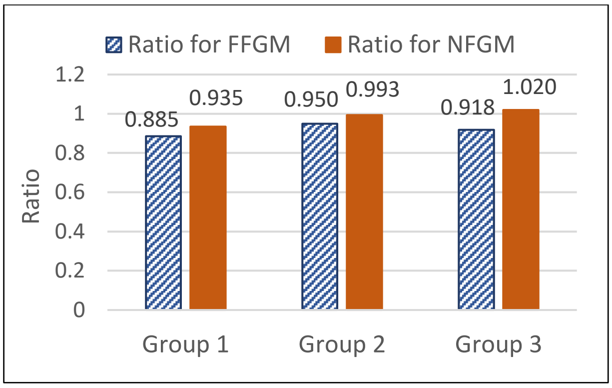

Figure 6.7. Bar Chart of A_p/V_p-T_c and T_p-T_c relationship for FFGM & NFGM for verification purpose.

6.4. Final Form of the Proposed Minimum Restoring Force Equations

The restoring force equations derived earlier include the parameters A_p/V_p and T_p, which are unpractical to use while checking the minimum restoring force requirement of seismic isolated structures. Therefore, the parameters A_p/V_p and T_p, in the restoring force equations are replaced by the corner period T_c of the design spectrum using the relationship between A_p/V_p and T_c for FFGM and T_p and T_c for NFGM. Accordingly, substituting Eq.25 into Eq.14 and simplifying, the final form of the minimum restoring force equation to limit the residual displacement for FFGM takes the following form,

$$T_d < \frac{(mA_p)^{\left(\frac{16}{25}\right)} \; T_c^{\left(\frac{1}{3}\right)}}{Q_d^{\left(\frac{1}{2}\right)}} \tag{27}$$

Similarly, substituting Eq.25 into Eq.17 and simplifying, the final form of the restoring force equation to limit the isolation system displacement for FFGM is expressed as follows;

$$T_d < \frac{550 \times 10^6 \, Q_d}{(mA_p)^{\left(\frac{33}{10}\right)} \; T_c^{\left(\frac{15}{4}\right)}} \tag{28}$$

For NFGM, substituting the relationship between T_p and T_c (Eq.26) into Eqs.20 and 21 and simplifying, the final form of the minimum restoring force equations to limit the residual and maximum displacements are obtained and presented in Eqs. 29 and 30 respectively;

$$T_d < \frac{0.17(mA_p)^{\left(\frac{21}{25}\right)}\, T_c^{\left(\frac{14}{25}\right)}}{Q_d^{\left(\frac{13}{25}\right)}} \tag{29}$$

$$T_d < \frac{235 \times 10^6\, Q_d^{\left(\frac{11}{20}\right)}}{(mA_p)^{\left(\frac{13}{5}\right)}\, T_c^{\left(\frac{8}{5}\right)}} \tag{30}$$

The smaller of T_d obtained from Eqs.27 and 28 for FFGM and Eqs.29 and 30 for NFGM shall be used to determine the upper limit of the post-elastic period of the seismic isolation system to ensure reasonable levels of residual and maximum isolation system displacements. It is noteworthy that the numerators of Eqs.28 and 30 may yield quite large numbers and if such large numbers are not counterbalanced by the denominators of the same equations, very large limits for the post elastic periods may be obtained. This indicates that the limit on the residual displacement (Eqs. 27 and 29) rather than the maximum displacement of the isolation system govern the restoring force requirement. However, in the case of seismic isolation systems with low characteristic strength subjected to ground motions with intense, long duration acceleration pulses (those with large T_c), the limit imposed on the maximum displacement (Eqs.28 and 30) governs the restoring force requirement.

The graphical representation of Eqs.27 to 30 are presented in Figure 6.8(a) and Figure 6.8(b) for FFGM and in Figure 6.8(c) and (d) for NFGM. As observed from the figures, T_d's for limiting the residual displacement (continuous lines) generally govern the design for seismic isolated structures with larger characteristic strength subjected to ground motions with smaller intensity and for stiffer soil conditions. For instance, as observed from Figure 6.8(a) for stiffer soil conditions (T_c=0.3 s), the T_d for limiting the residual displacement govern the post-elastic period limit for a wide range of mA_p/Q_d ratios (up to 42). However, for softer soil conditions (T_c=1.1 s), the T_d for limiting the residual displacement govern the post-elastic period limit up to mA_p/Q_d=11. The observations are similar in the case of other figures (Figure 6.8(b)-(d)). This clearly proves the necessity of providing upper limits for the post-elastic period of seismic isolated structures considering both the residual and maximum isolation system displacements.

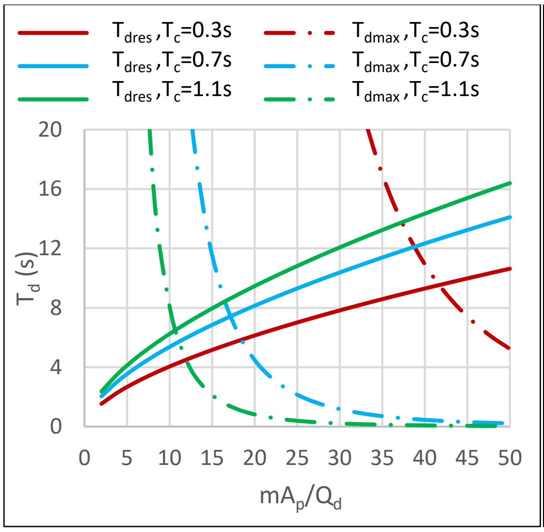

(a)

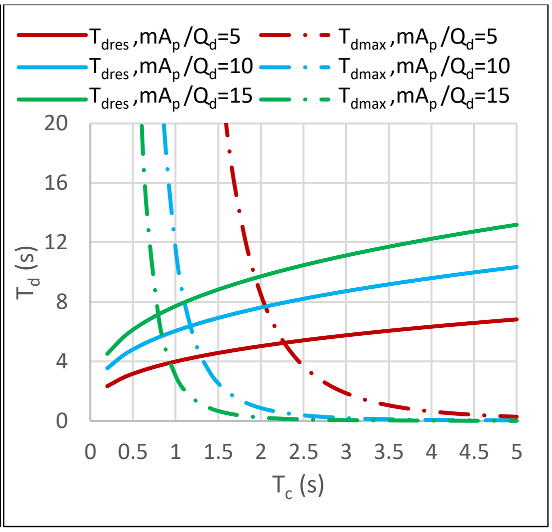

(b)

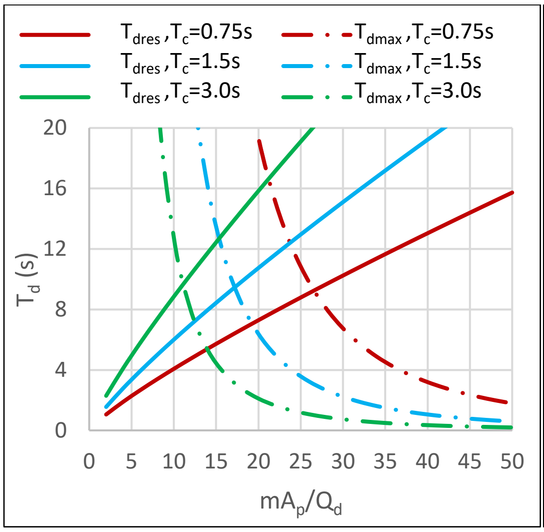

(c)

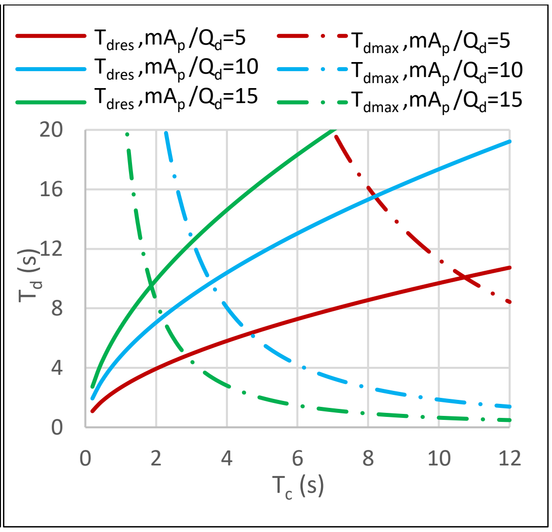

(d)

Figure 6.8. Comparison Eqs. 27 and 28 as a function of (a) mA_p/Q_d & (b) T_c, comparison of Eqs. 29 and 30 as a function of (c) mA_p/Q_d & (d) T_c

CHAPTER 7

COMPARISON OF EC-8, AASHTO AND THE PROPOSED RESTORING FORCE EQUATIONS WITH THE ANALYSIS RESULTS

In this part, the proposed restoring force equations together with those of AASHTO [1] and EC-8 [2] are comparatively assessed with respect to the NLTHA results.

First, the restoring force equation of EC-8 [2] (Eq.5) is tested with respect to the NLTHA results. As the restoring force requirement of EC-8 [2] is based on limiting the residual displacement, the NLTHA results in terms of the d_{res}/d_{max} ratios are plotted as a function of the d_{max}/d_{rm} ratio in Figure 7.1(a) and Figure 7.1(b) for FFGM and NFGM respectively. Then, two power functions are fitted to the data points for FFGM and NFGM by a minimum least square curve fitting procedure. As observed from the figures, for $d_{max}/d_{rm} = 0.5$, the corresponding d_{res}/d_{max} ratios are 0.09 and 0.10. That is, the residual displacements of the seismic isolation system subjected to FFGM and NFGM are 9% and 10% of their maximum displacements respectively. This clearly indicates that the restoring force equation of EC-8 [2] works quite well in limiting the residual displacements. Although the restoring force equation of EC-8 [2] is not intended for limiting the maximum displacement, it is still tested to assess its ability to limit the maximum displacements. For this purpose, first the restoring force equation of EC-8 [2] is rearranged to obtain the following relationship; $d_{rm}/d_{max} < 2.0$. Then, the NLTHA results in terms of the d_{max} are plotted as a function of the d_{rm}/d_{max} ratio in Figure 7.2(a) and (b) for FFGM and NFGM respectively. Then, two power functions are fitted to the data points for FFGM and NFGM by a minimum least square curve fitting procedure. As observed from the figures, for $d_{rm}/d_{max} < 2.0$, the isolation system displacements could be unreasonably large. This clearly indicates that although the restoring force equation of EC-8 [2] works well in limiting the residual displacements, it fails to limit the maximum displacements. Accordingly, for unreasonably large values of maximum displacements, the EC-8 [2] code provision allows for larger residual displacements as long as the d_{res}/d_{max} ratios is kept about 0.10. Thus, this requirement alone does not ensure a sufficient restoring force capability for a seismic isolated structure. For instance, according to code provisions, for an isolator displacement of 1000 mm, the residual displacement may be as large as 100 mm. Such a displacement is too large to ensure the serviceability of a structure after a potential earthquake. Therefore, it is clear that a limit on the maximum displacement is also required.

As mentioned earlier, AASHTO [1] presents two restoring force requirements. The first requirement limits the residual displacements by an equation (Eq.2), which is a function of the post-elastic stiffness, the maximum displacement and the structure weight. Accordingly, the NLTHA results in terms of d_{res}/d_{max} ratios are plotted as a function of the parameters of the first requirement of AASHTO [1] in terms of $(k_d \times d_{max})/W$ in Figure 7.3. As observed from the figure, for $(k_d \times d_{max})/W$=0.025, the corresponding d_{res}/d_{max} ratios are 0.11 and 0.14. That is, the residual displacements of the seismic isolation system subjected to FFGM and NFGM are 11% and 14% of their maximum displacements respectively. Although larger than those of EC-8 [2], the residual displacement limits of AASHTO [1] based on d_{res}/d_{max} ratios of 0.11 and 0.14 may be considered as acceptable. The second requirement of AASHTO [1], which is presented in Eq.3, states that the post-elastic period of a seismic isolated structure should be smaller than 6 seconds. When the first and the second requirements of AASHTO [1] are combined (Eq.4), it appears that the maximum isolation system displacements are also limited to 224 mm.

To test the effectiveness of the restoring force requirements of EC-8 [2] and AASHTO [1] compared to those proposed in this research study, the entire pool of NLTHA results of the seismic isolated structures considered in this research study is used. For this purpose, from the entire pool of NLTHA data (residual and maximum displacements), those that satisfy EC-8 [2] and AASHTO [1] restoring force requirements as well as the requirements proposed in this research study are identified.

Next, the identified residual and maximum displacement data that satisfy AASHTO [1], EC-8 [2] and the proposed restoring force requirements are plotted as a function of T_d in Figure 7.4 and Figure 7.5 for FFGM and NFGM respectively. As observed from the figures, in the case of AASHTO [1] and EC-8 [2], residual and maximum displacements for FFGM in excess of 1.0 m and 5.0 m respectively as well as residual and maximum displacements for NFGM in excess of 1.8 m. and 9.9 m respectively are allowed although the code restoring force requirements are satisfied. However, when the restoring force requirements proposed in this research study are applied, the residual and maximum displacements are respectively limited to 0.13 and 1.0 m for FFGM and 0.11 and 1.7 m for NFGM. The averages of the data satisfying the proposed equations are respectively calculated as 0.013 and 0.245 m for the residual and maximum displacements for FFGM and 0.015 and 0.366 m for NFGM. The results presented in Figure 7.4 and Figure 7.5 clearly proves that the restoring force requirements proposed in this research study produce more reasonable residual and maximum displacements. Although in the proposed research study the maximum displacement is intended to be limited to 600 mm, in some limited number of cases (4% of the data points for FFGM and 19% for NFGM), larger values are obtained due to the scatter of data used in the estimation of the threshold value of the displacements.

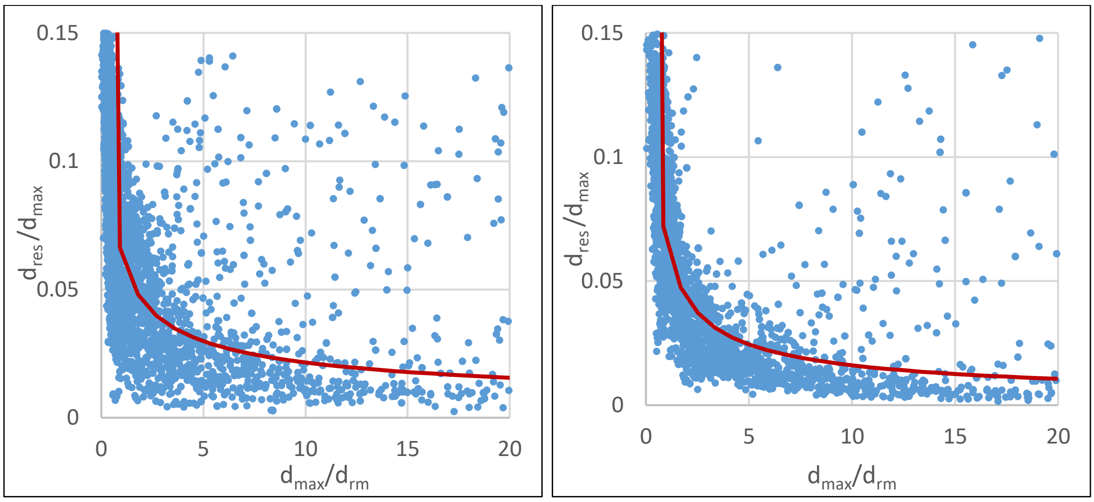

(a) (b)

Figure 7.1. Plots for d_{max}/d_{rm} and d_{res}/d_{max} for (a) FFGM (b) NFGM

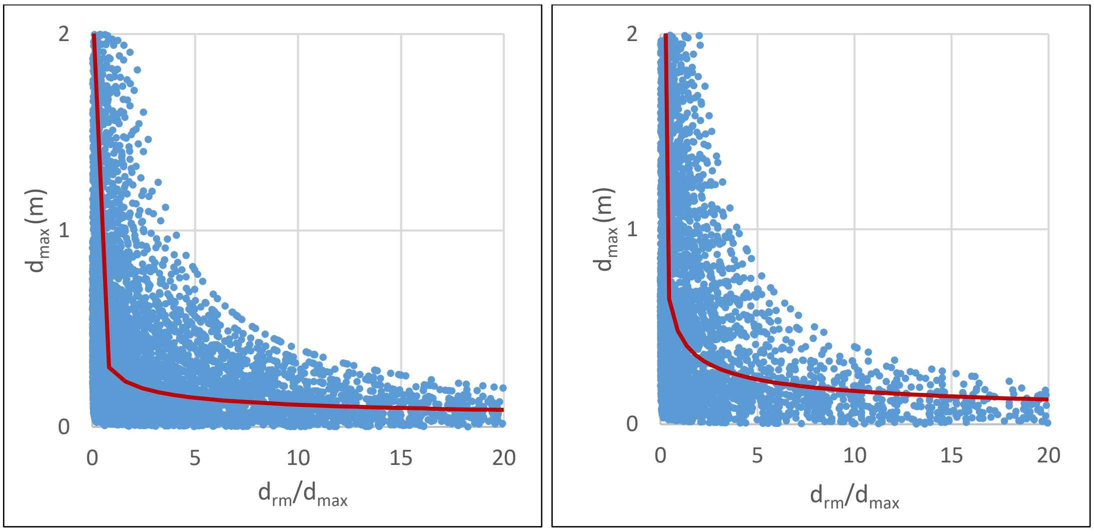

(a) (b)

Figure 7.2. Plots for d_{max} and d_{rm}/d_{max} for (a) FFGM (b) NFGM

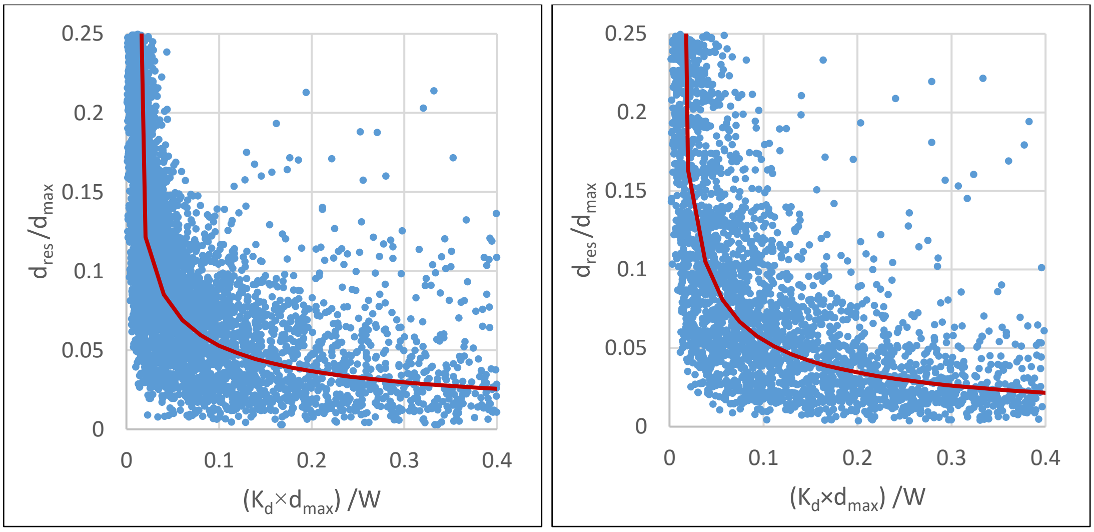

(a) (b)

Figure 7.3. Plots for $(K_d \times d_{max})$ /W and d_{res}/d_{max} for (a) FFGM (b) NFGM

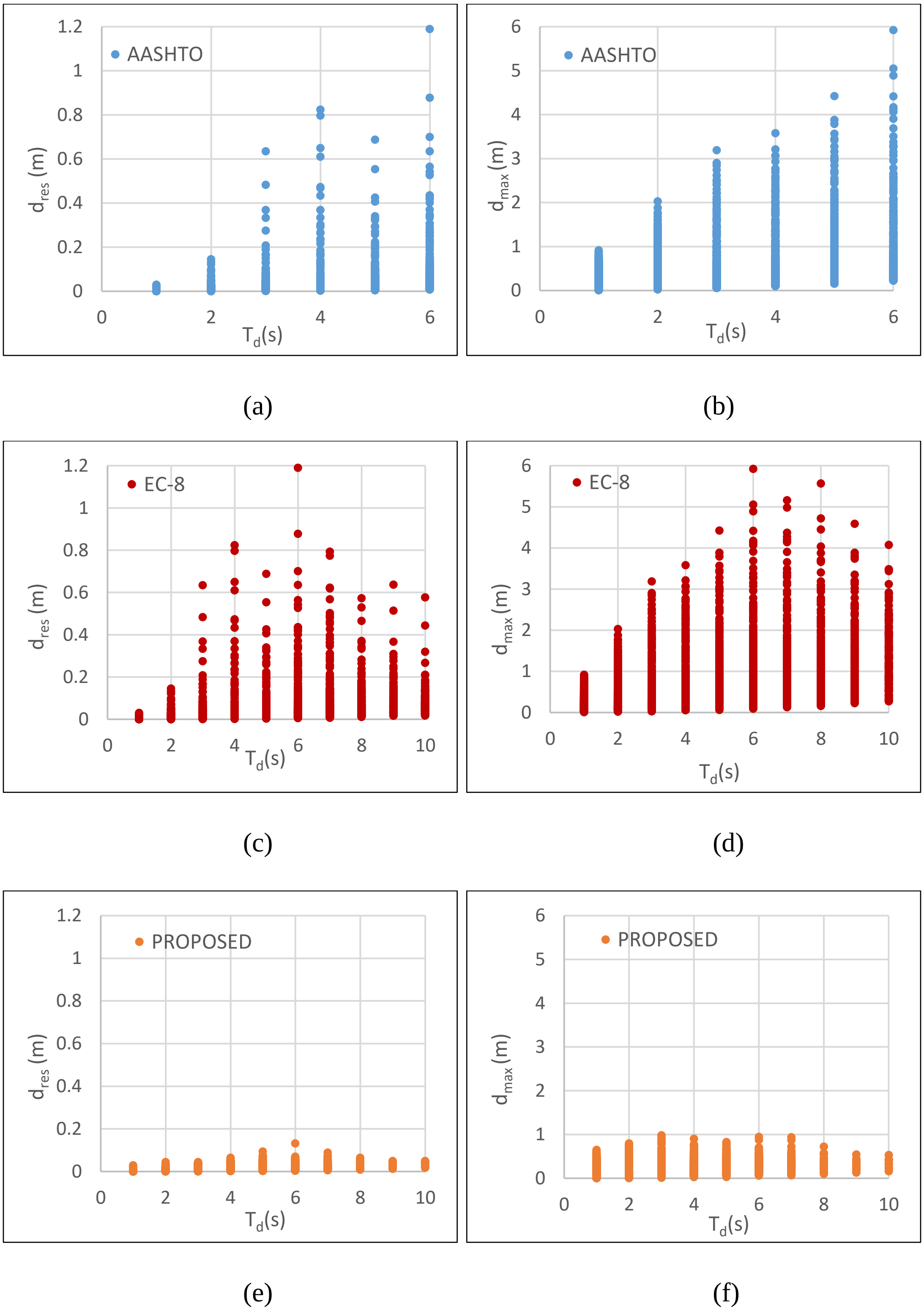

Figure 7.4. Comparison of the codes (a)&(b) AASHTO [1] ,(c)&(d) EC-8 [2] and (e)&(f) the proposed equations with the analysis results for FFGM.

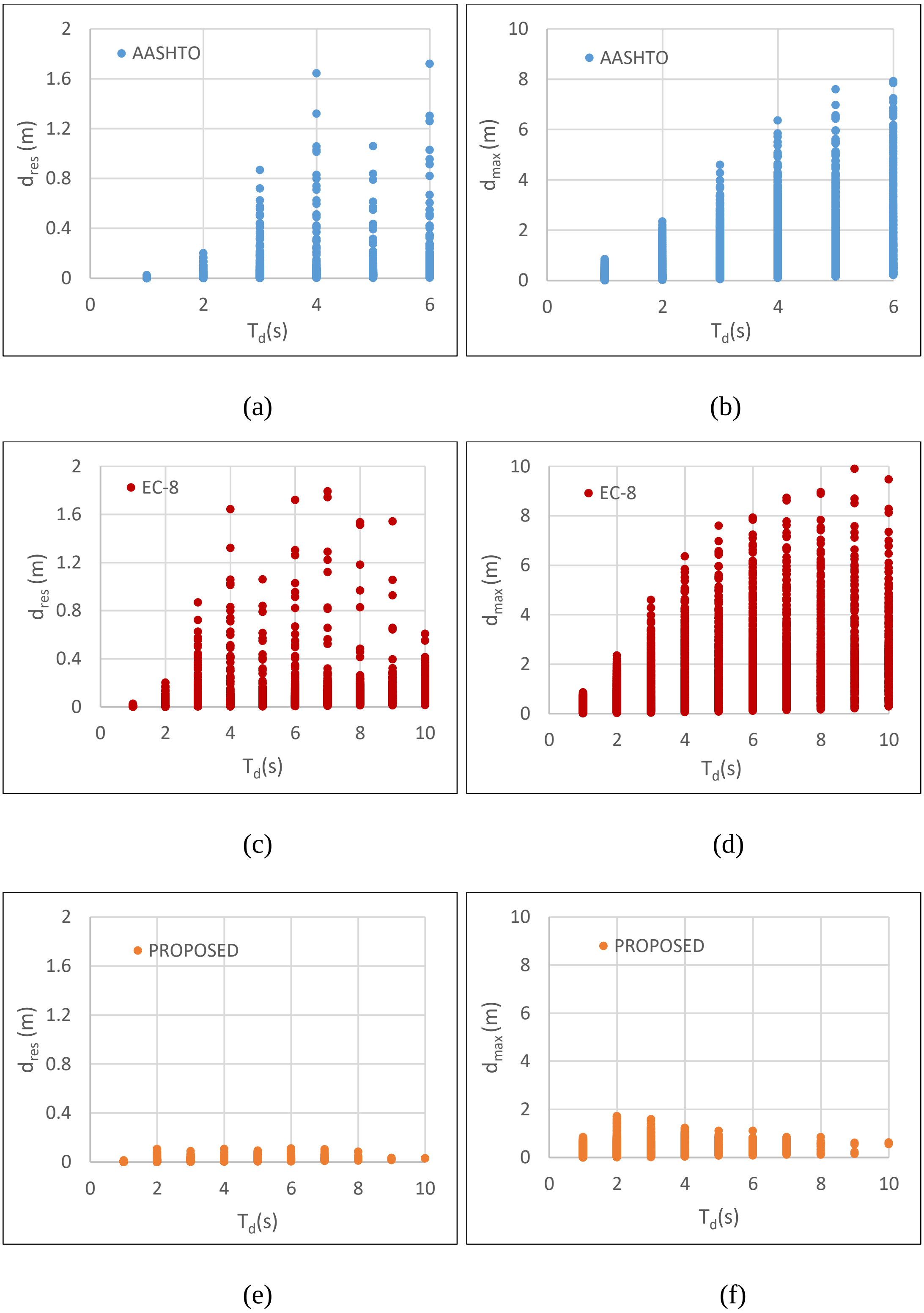

Figure 7.5. Comparison of the codes (a)&(b) AASHTO [1] ,(c)&(d) EC-8 [2] and (e)&(f) the proposed equations with the analysis results for NFGM.

CHAPTER 8

CONCLUSIONS

In this research study, a new set of restoring force equations are proposed for seismic isolated structures subjected to FFGM and NFGM. For this purpose, 110 FFGM and 49 NFGM are selected. Then, NLTHA of SDOF seismic isolated structures are performed using the selected ground motions to obtain their residual and maximum displacements. The analyses are repeated for an extensive range of parameters including peak ground acceleration, A_p, characteristic strength, Q_d and post elastic period, T_d, of the isolation system. Next, nonlinear regression analyses are performed on the NLTHA results to formulate the residual and maximum displacements as functions of the parameters considered in the analyses. These equations are then used to formulate the upper limits of T_d (restoring force equations) to ensure reasonable levels of residual and maximum isolator displacements. The restoring force equations proposed in this research study are then compared with those of AASHTO [1] and EC-8 [2]. Followings are the conclusions deduced from this research study;

i. Equations to calculate the residual and maximum displacements of SDOF seismic isolated structures are developed through regression analyses of the data obtained from parametric NLTHA conducted as part of this research study. These equations may be used to obtain approximate values of residual and maximum displacements of seismic isolated structures for preliminary design purposes.

ii. The NLTHA results revealed that for both FFGM and NFGM, the maximum isolation system displacement increases with increasing values of mA_p and T_d, but decreases, with increasing values of Q_d and A_p/V_p for

FFGM. For NFGM, the observations are similar except for T_p, where the maximum displacement increases with increasing T_p.

iii. It is also observed that for both FFGM and NFGM, the residual displacement increases with increasing values of mA_p, Q_d and T_d, but decreases, with increasing values A_p/V_p for FFGM. For NFGM, the observations are similar except for T_p, where the residual displacement increases with increasing T_p.

iv. The plot of the d_{res}/d_{max} ratio as a function of a parameter representing the isolator and ground motion characteristics indicates that at a certain threshold value, the variation of the d_{res}/d_{max} ratio become asymptotic to the vertical axis. This threshold value of d_{res}/d_{max} ratio is estimated as 0.1. Thus, limiting the d_{res}/d_{max} ratio to 0.1 is essential to obtain reasonable levels of residual displacements. Both the EC-8 [2] and the restoring force equations proposed in this study to limit the residual displacements are based on d_{res}/d_{max} = 0.1. However, it appears that in the case of AASHTO [1], d_{res}/d_{max} ratios of 0.11 and 0.14 are considered for FFGM and NFGM respectively.

v. The plot of d_{max} as a function of a parameter representing the isolator and ground motion characteristics indicates that at a threshold displacement value of around 600 mm, the variation of d_{max} become asymptotic to the vertical axis. Consequently, formulating the restoring force requirement based on d_{max}=600 mm or a smaller value may produce reasonable levels of isolation system displacements.

vi. It is observed that restoring force equations developed as part of this study for limiting the residual displacements generally govern the design for seismic isolated structures with larger characteristic strength subjected to ground motions with smaller intensity and for stiffer soil conditions. For other cases, restoring force equations developed for limiting the maximum displacements govern the design of seismic isolated structures.

vii. As NFGM produce larger residual and maximum seismic isolation system displacements than those of FFGM, it is important to differentiate between such ground motions as in the case of the restoring force equations proposed in this study. Nevertheless, neither AASHTO [1] nor EC-8 [2] make any distinction between NFGM and FFGM in their restoring force equations. Furthermore, the restoring force requirement of EC-8 is solely based on limiting the residual displacements and no limitation is imposed on the maximum isolation system displacement.

viii. The restoring force requirements of ASSHTO [1], EC-8 [2] and those proposed in this research study are comparatively assessed using the pool of residual and maximum displacement data obtained from parametric NLTHA. It is observed that in the case of AASHTO [1] and EC-8 [2], residual and maximum displacements in excess of respectively 1.8 m and 9.9 m are allowed although the code restoring force requirements are satisfied. However, when the restoring force requirements proposed in this research study are applied, the residual and maximum displacements are respectively limited to 0.13 and 1.7 m. Thus, the restoring force requirements proposed in this research study produce more reasonable residual and maximum displacements. Although the maximum displacement is intended to be limited to 600 mm in the proposed restoring force equations, some limited number of larger values are obtained due to the scatter of the data used in the estimation of the threshold value of the displacements.

ix. An important correlation is derived as part of this research study between A_p/V_p and the second corner period, T_c of the response spectrum for FFGM as well as T_p and T_c for NFGM. These relationships may be helpful in various analyses and design applications since design response spectrum is an easily accessible tool to design engineers.

REFERENCES

[1] AASHTO Guide Specifications for Seismic Isolation Design, American Association of State Highway and Transportation Officials, Washington, D.C, 2014.

[2] CEN. Eurocode 8: Design of Structures for Earthquake Resistance – Part 2: Bridges, EN1998-2:2005. Bruxelles, Belgium: European Committee for Standardization; 2011.

[3] ASCE 7-16 Minimum Design Loads and Associated Criteria for Buildings and Other Structures, American Society of Civil Engineers New York, NY, 2016

[4] European Standard _EN 15129: Anti-Seismic Devices _Brussels, 2010

[5] Medeot R. Re-Centering Capability Evaluation of Seismic Isolation Systems Based on Energy Concepts. In: Proceedings of the 13th World Conference on Earthquake Engineering Paper 3106. Canada, Vancouver; 2004.

[6] Tsopelas P, Okamoto S, Constantinou MC, Ozaki D, Fujii S NCEER-TAISEI Corporation Research Program on Sliding Seismic Isolation Systems for Bridges-Experimental and Analytical Study of Systems Consisting of Sliding Bearings, Rubber Restoring Force Devices And fluid Dampers. Technical Report NCEER-94-0002, University of New York at Buffalo, Buffalo, NY;1994

[7] American Association of State Highways and Transportation Officials (AASHTO). Guide Specifications for Seismic Isolation Design. Washington, D.C, 1991

[8] Katsaras CP, Panagiotakos TB, Kolias B. Restoring capability of bilinear hysteretic seismic isolation systems. Earthq Eng Struct Dyn 2008; 37:557–575.

[9] American Association of State Highways and Transportation Officials (AASHTO). Guide Specifications for Seismic Isolation Design—Interim 2000, Washington, D.C, 2000.

[10] Cardone D, Gesualdi G, Brancato P. Restoring Capability of Friction Pendulum Seismic Isolation Systems. Bull Earthq Eng 2015;13(8):2449-80.

[11] Pacific Earthquake Engineering Research Center. PEER Strong Motion Database. Available from: https://ngawest2.berkeley.edu/spectras/new.

[12] Baker JW. Quantitative classification of near-fault ground motions using wavelet analysis. Bull Seismol Soc Am 2007;97(5):1486–1501

[13] SAP 2000 V.17 Computers and Structures INC., Berkeley, CA, USA, 2017

[14] Kawashima K, MacRae GA, Hoshikuma J, Kazuhiro N. Residual displacement response spectrum. J Struct Eng (ASCE) 1998;124(5):523–530.

[15] FHWA (Federal Highway Administration). LRFD Seismic Analysis and Design of Bridges Reference Manual NHI Course No: 130093 and 130093A, FHWA-NHI-15-004, FHWA, Washington, D.C.,2014.